

Dynamics of 3-planet systems: orbital stability/chaos indicators

By

Konstantinos Foutzopoulos

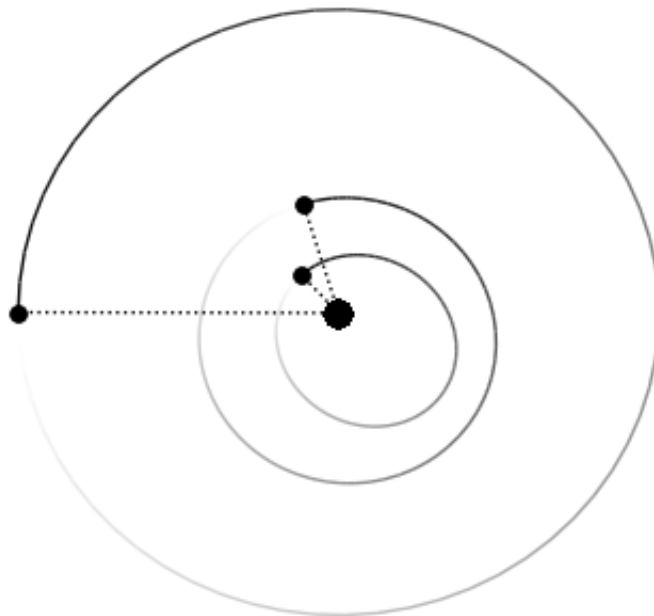
A thesis
submitted in partial fulfillment of the
requirements for the degree of

Master of Science in Computational Physics

at

Aristotle University of Thessaloniki
Department of Physics

Oct, 2023



Thesis supervisor
George Voyatzis, Professor

ABSTRACT

Predicting the stability of a system has paramount importance in dynamical systems and celestial mechanics. One of the hot topics in the last few decades is the stability of planetary systems that seem to exist with very different configurations. Actually the stability problem and evolution of planetary systems is reduced to the the stability of classical N -body problem which is a chaotic dynamical system. A comparative study of some chaos indicators, utilizing deviation vectors taken by integrating the variational equations, is performed applying them to the 3-planet system HD 82943, after presenting the necessary theoretical background regarding dynamical systems, celestial mechanics, and that of variational equations and the chaos indicators, specifically LCN, DFLI, MEGNO, SALI, and RLI.

ΠΕΡΙΛΗΨΗ

Δυναμική συστημάτων 3-πλανητών – Δείκτες ευστάθειας/χάους τροχιών

Η πρόβλεψη της ευστάθειας ενός συστήματος είναι κύριας σημασίας στα δυναμικά συστήματα και την ουράνια μηχανική. Ένα από τα πιο καυτά θέματα των τελευταίων δεκαετιών είναι η πρόβλεψη της ευστάθειας πλανητικών συστημάτων τα οποία εμφανίζονται να υπάρχουν για πολύ διαφορετικές διαμορφώσεις. Πραγματικά το πρόβλημα ευστάθειας και η εξέλιξη των πλανητικών συστημάτων ανάγεται στην ευστάθεια του κλασσικού προβλήματος των N -σωμάτων το οποίο είναι ένα χαοτικό δυναμικό σύστημα. Μια συγκριτική μελέτη κάποιων χαοτικών δεικτών, χρησιμοποιώντας διανύσματα απόκλισης τα οποία λαμβάνονται ολοκληρώνοντας τις εξισώσεις μεταβολών, πραγματοποιείται εφαρμόζοντας αυτούς στο σύστημα 3-πλανητών HD 82943, αφότου παρουσιαστεί το απαραίτητο θεωρητικό υπόβαθρο σχετικά με δυναμικά συστήματα, ουράνια μηχανική, και αυτό των εξισώσεων μεταβολών και χαοτικών δεικτών, συγκεκριμένα LCN, DFLI, MEGNO, SALI, και RLI.

ΕΚΤΕΤΑΜΕΝΗ ΠΕΡΙΛΗΨΗ

An extensive abstract written in Greek due to thesis requirements.

Δυναμικό σύστημα είναι ένα σύστημα το οποίο περιγράφεται από ένα αριθμό χρονοεξαρτημένων μεταβλητών, δηλαδή το σύστημα έχει μια εξέλιξη στο χρόνο. Η εξέλιξη των μεταβλητών και κατά συνέπεια του συστήματος περιγράφεται από ένα κανόνα που σε χρονική στιγμή t καθορίζει τη κατάσταση σε χρονική $t + \delta t$. Ο αριθμός των μεταβλητών καθορίζει τη διάσταση του συστήματος και ο χώρος στον οποίο αποτυπώνεται η εξέλιξη ονομάζεται χώρος φάσεων (ή καταστάσεων). Ένα συνεχές δυναμικό σύστημα περιγράφεται από μια ροή και ένα αντίστοιχο σύστημα διαφορικών εξισώσεων.

Μια σημαντική κατηγορία δυναμικών συστημάτων είναι τα Χαμιλτονιανά συστήματα των οποίων η κίνηση καθορίζεται πλήρως από τη συνάρτηση Χάμιλτον μέσω του συμπλεκτικού φορμαλισμού. Τα Χαμιλτονιανά συστήματα είναι ολοκληρώσιμα εάν υπάρχει επαρκής αριθμός ολοκληρωμάτων, δηλαδή ποσοτήτων που διατηρούνται σταθερές. Μη-ολοκληρώσιμα συστήματα εμφανίζουν χάος.

Χάος, όπως παρατηρείται στα δυναμικά συστήματα, είναι το φαινόμενο που χαρακτηρίζεται από περίτεχνες, απρόβλεπτες, και απεριοδικές συμπεριφορές. Εμφανίζεται σε συστήματα που εμφανίζουν μη-γραμμικότητα με αποτέλεσμα πολύπλοκων, φαινομενικά τυχαίων τροχιών μετά από κάποιο χρόνο. Δεν υπάρχει ακριβής ορισμός του χάους. Ένας κοινός ορισμός κατά Devaney ορίζει ως χάος ένα σύστημα με ευαίσθητη εξάρτηση στις αρχικές συνθήκες, τοπολογική μεταβατικότητα, και πυκνές περιοδικές τροχιές στο χώρο φάσεων. Οι τεχνικές εύρεσης χάους χωρίζονται σε γραφικές όπως τομές Poincaré και αριθμητικής ανάλυσης των τροχιών όπως οι δείκτες που βασίζονται στην εξέλιξη των διανυσμάτων απόκλισης.

Καταφεύγουμε σε αριθμητικές μεθόδους διότι οι διαφορικές εξισώσεις εν γένει δεν λύνονται. Μια μέθοδος που επιτρέπει υψηλής ακρίβειας λύσεις με ελάχιστο υπολογιστικό κόστος είναι η Bulirsch-Stoer που συνδυάζει τρεις ιδέες. Συγκεκριμένα τη παρεμβολή Richardson, μια μέθοδο προσαρμογής (συναρτησιακή ή πολυωνυμική παρεμβολή), και τη τροποποιημένη μέθοδο μέσου βήματος (ολοκληρωτής).

Το πρόβλημα πρόβλεψης της κίνησης κάποιων σωμάτων υπό την αμοιβαία βαρυτική τους αλληλεπίδραση ορίζει το περίφημο πρόβλημα των N -σωμάτων. Οι εξισώσεις κίνησης στη Χαμιλτονιανή προσέγγιση προκύπτουν θεωρώντας το βαρυτικό δυναμικό του κάθε σώματος υπό την επήρεια των άλλων σωμάτων, το οποίο μας επιτρέπει να γράψουμε τη Χαμιλτονιανή του συστήματος και η οποία μέσω του συμπλεκτικού φορμαλισμού δίνει τις εξισώσεις κίνησης. Το σύστημα έχει 10 ολοκληρώματα τις κίνησης και συνεπώς για $N > 2$ είναι μη-ολοκληρώσιμο. Το πλανητικό πρόβλημά είναι το πρόβλημα των $(N + 1)$ -σωμάτων όπου το 1 είναι πολύ βαρύτερο από τα υπόλοιπα και στο οποίο μας ενδιαφέρει η κίνηση των υπολοίπων N .

Έχοντας τις εξισώσεις κίνησης μπορούμε να βρούμε τις εξισώσεις μεταβολών, των οποίων η επίλυση δίνει τη τροχιά ενός διανύσματος, αποκαλούμενο διάνυσμα απόκλισης, που περιγράφει μια διαταραχή της κανονικής τροχιάς που εξελίσσεται εφαιπτομενικά της ροής. Κατά την αριθμητική ολοκλήρωση οι εξισώσεις μεταβολών μιας δίνουν πληροφορία σχετικά με την (1η-τάξης) ευστάθεια κατά το χρόνο ολοκλήρωσης.

Έχοντας την εξέλιξη του διανύσματος απόκλισης και γνωρίζοντας πως το χάος χαρακτηρίζεται από ευαίσθητη εξάρτηση στις αρχικές συνθήκες μπορούμε να υπολογίσουμε τη μεταβολή του διανύσματος απόκλισης. Πάνω σε αυτή την ιδέα στηρίζονται οι χαοτικοί δείκτες γνωστοί και ως δείκτες μεταβολών. Εφαρμογή αυτών των δεικτών σε ένα πλέγμα αρχικών συνθηκών για το σύστημα που μελετάται μας δίνει ένα χάρτη ευστάθειας.

Σε ένα πλανητικό σύστημα οι δυναμικές παράμετροι είναι τα τροχιακά στοιχεία και οι μάζες των πλανητών. Η παρούσα εργασία ερευνά τους δείκτες χαοτικότητας μεταβάλλοντας τα στοιχεία του εξωτερικού πλανήτη σε ένα σύστημα 3-πλανητών.

TABLE OF CONTENTS

ABSTRACT	3
ΕΚΤΕΤΑΜΕΝΗ ΠΕΡΙΛΗΨΗ	5
PROLOGUE	9
1. DYNAMICAL SYSTEMS	11
1.1. Introduction	11
1.2. Hamiltonian systems	12
1.3. Chaos	13
1.4. Numerical integration methods	14
1.4.1. Bulirsch-Stoer	14
1.4.2. Symplectic	15
1.5. Showcasing an example system	16
2. CELESTIAL MECHANICS	23
2.1. Orbits	23
2.2. Equations of motion	24
2.3. N -body problem	25
2.4. Planetary problem	26
2.5. Showcasing in 3-planet system	27
3. VARIATIONAL EQUATIONS (VEqs)	29
3.1. VEqs of dynamical systems	29
3.2. VEqs of Hamiltonian systems	30
3.3. VEqs of N -body problem	31
3.4. VEqs of planetary problem	32
3.5. Showcasing in example system	33
4. STABILITY ANALYSIS	37
4.1. Chaos indicators	37
4.1.1. LCE/LCN	37
4.1.2. FLI/DFLI	38
4.1.3. OFLI/2	39
4.1.4. MEGNO	39
4.1.5. SALI/GALI	41
4.1.6. RLI	42
4.2. Showcasing in example system	43
4.2.1. LCE/LCN	44
4.2.2. FLI/DFLI	46
4.2.3. MEGNO	48
4.2.4. SALI	49
4.2.5. RLI	51
5. NUMERICAL INTEGRATIONS	55

CONCLUSIONS	67
APPENDIX A. SOURCES	67
A.1. Variational equations	70
A.2. Chaos indicators	77
BIBLIOGRAPHY	77

PROLOGUE

A dynamical system is a system which evolves over time and its evolution is depicted on a phase (or state) space. Qualitatively there's a need to know its asymptotic properties, what happens to it after a long time period. Knowing a particular orbit it's natural to wonder what happens when there's a small change to its initial conditions.

Stability theory arises to answer the question of whether nearby (i.e. perturbed) orbits will remain close or diverge or converge. To numerically investigate the stability of dynamical systems, frequency map analysis (or newer variations, such as spectral analysis of orbital elements) or integration of variational equations and computation of chaos indicators can be used.

A number of celestial bodies interacting gravitationally, forming what is known as the N -body problem, are described by a dynamical system. Currently the number of exoplanets and systems those are arranged in exceed 5000 and 4000 respectively¹. Numerically integrating and predicting the stability of integrated orbits allows to restrict their data and whence improve the accuracy of studies that use that.

Overall, studying the N -body problem contributes to our understanding of celestial mechanics, planetary systems, and exoplanets, while also offering a testing ground for mathematical and computational techniques, with implications for space missions and astronomical observations.

The thesis is split into four chapters and one where the numerical integrations for a 3-planet system are shown, on which the comparative study and conclusions are based. The theoretical chapters present the necessary background for understanding (i) dynamical systems and utilized numerical integration scheme, (ii) the planetary problem and its equations of motion, (iii) the variational equations of the previous problem, (iv) chaos indicators.

We also show some specific examples of the presented theory in every theoretical chapter, and how the equations required for studying those examples can be extracted computationally using the computer algebra system Maxima. In the appendix parts of the code used for the numerical integrations are provided to complement the presented theory.

Acknowledgments. The author thanks his thesis supervisor and teacher, prof. George Voyatzis, for suggesting the thesis topic and their patience in the longer than expected time it took for completion. Some results presented in this work have been produced using AUTH HPC infrastructure.

1. As of 30 Oct 2023 based on data from exoplanet.eu there're 5521 confirmed exoplanets arranged in 4070 systems, 885 systems having >1 planets (noting that is 588 of 2 and 177 of 3 planets).

CHAPTER 1

DYNAMICAL SYSTEMS

1.1. INTRODUCTION

Dynamical systems, of which origins lie in the early mathematical and physical inquiries into behaviors of mechanical systems and celestial motion, constitute a foundational and interdisciplinary framework for investigating the temporal evolution of diverse phenomena. Their theory describe the behavior of systems as they transition from one state to another over time, under the influence of internal dynamics or external forces.

Formally, a dynamical system is a mathematical or/and physical system of which the state is fully described by finite independent variables x_i (if physical $x_i \in \mathbb{R}$) that evolve in time $t \in \mathbb{R}$, meaning the variables are time dependent, that is $x_i = x_i(t)$ [1][2]. Their time evolution, and by extension the system, is described by a rule $x_i \mapsto x_i'$ that for a moment t defines the state of the system at moment $t + \delta\tau$. The number of variables n define the dimension of the system and the n -dimensional space $E \subseteq \mathbb{R}^n$ defined from those is called phase space (or state space).

Symbolically, a dynamical system is defined as a flow (or map) $\varphi(\mathbf{x}, t)$ on phase space

$$\varphi: \mathbb{R} \times E \rightarrow E \tag{1.1}$$

that moves (or maps) a point \mathbf{x} at time t to a point \mathbf{x} at t' [1][2]. The time t can be either continuous or discrete, in which case $t = t_0 + k\delta\tau$. If the flow doesn't depend explicitly on time, that is if $\partial_t \varphi = 0$, then the system is called autonomous whereas if it does is called non-autonomous. If the rule doesn't include any randomness the system is deterministic whereas if it does is stochastic.

A continuous dynamical flow can be described by the differential equations

$$\frac{d\mathbf{x}}{dt} = \mathbf{f}(\mathbf{x}, t) \Leftrightarrow \frac{dx_i}{dt} = f_i(x_j, t) \tag{1.2}$$

whereas a discrete map by the equations

$$\mathbf{x}^{(k+1)} = \mathbf{f}(\mathbf{x}^{(k)}, k) \Leftrightarrow x_i^{(k+1)} = f_i(x_j^{(k)}, k) \tag{1.3}$$

Given an initial state $\mathbf{x}_0 = \mathbf{x}(t_0)$ the dynamical system forms an initial value problem. The points representing the time evolution of an initial state in the case of continuous systems define a *trajectory*, a continuous curve, whereas in the case of discrete systems define an *orbit*, a set of discrete points in the phase space.

A dynamical system is called integrable if it has sufficiently many conserved quantities (also called *first integrals* or *integrals of motion*), presence of algebraic geometry, and the ability to give explicit solutions. That is the system can be solved in some way. One way this can happen is if the flow of the vector field can be constructed analytically. However, this can almost never be done (in terms of elementary functions).

The equations f_i define the system's vector field that describe the motion on the phase space. The f_i are defined in space (\mathbf{x}, t) called the extended phase space. Assuming that the f_i and their first derivatives are continuous in the open subset of (\mathbf{x}, t) the solutions are unique.

A periodic orbit constitutes a special type of solution for a dynamical system. It's one which repeats itself in time. We define periodic orbit the solution $\gamma(t; x_0) = \varphi_t(x_0)$ for which it holds

$$\varphi_{t+T}(x_0) = \varphi_t(x_0) \Leftrightarrow \gamma(t+T) = \gamma(t) \quad (1.4)$$

1.2. HAMILTONIAN SYSTEMS

Named after the eminent mathematician and physicist W. R. Hamilton, these systems are characterized by their conservation of energy and symplectic structure, offering an elegant framework for understanding the behavior of physical systems. They represent a distinguished class of dynamical systems that play a pivotal role in many scientific disciplines.

Formally, these [1][3] are systems of which the time evolution is described fully by the Hamilton function (also called simply Hamiltonian) through the $2N$ equation system

$$\dot{z} = \mathbf{J} \cdot \nabla H \quad \mathbf{J} = \begin{pmatrix} \mathbf{0} & \mathbf{I} \\ -\mathbf{I} & \mathbf{0} \end{pmatrix} \quad (1.5)$$

and for canonically conjugate variables, $z = (\mathbf{p}, \mathbf{q})$, the equations split into two sets of N equations

$$\dot{\mathbf{q}} = \partial_{\mathbf{p}} H \quad \dot{\mathbf{p}} = -\partial_{\mathbf{q}} H \quad (1.6)$$

Here the N coordinates \mathbf{q} represent the system's configuration variables (e.g. positions) and the canonically conjugate \mathbf{p} , called momenta, represent the impetus gained by movement. Those equations represent the equations of motion of the system. If H does not contain t explicitly it's called autonomous and H is a constant of motion. Meaning

$$\dot{H} = \partial_{\mathbf{q}} H \dot{\mathbf{q}} + \partial_{\mathbf{p}} H \dot{\mathbf{p}} = 0 \Rightarrow H(\mathbf{q}, \mathbf{p}) = H(\mathbf{q}_0, \mathbf{p}_0) \quad (1.7)$$

If the equations are mechanical, the Hamiltonian is the total energy of the system and has the form

$$H = T(\mathbf{p}) + V(\mathbf{q}) = \sum_i \frac{p_i^2}{2m_i} + V(\mathbf{q}) \quad (1.8)$$

and the Hamilton equations become

$$\dot{\mathbf{q}} = \mathbf{p} \quad \dot{\mathbf{p}} = -\partial_{\mathbf{q}} V(\mathbf{q}) \quad (1.9)$$

As an historical note, the previous function is the one Hamilton showed could be used to derive Newton's equations for particles in a conservative field. This formulation gives a convenient restatement of Newton's system but shouldn't be regarded as just a simplification of it[3].

A $2N$ Hamiltonian system is integrable if there're N first integrals. There is a class of Hamiltonian systems, action-angle systems, whose solutions can be obtained analytically, and there is a well-accepted definition of integrability due to Liouville in which each integrable Hamiltonian is (locally) equivalent to these action-angle systems[3].

A Hamiltonian system is written in action-angle form if there is a set of canonical variables (θ, I) and such that H depends only upon the actions $H(I)$. In this case the equations of motion become

$$\dot{\theta} = \nabla H(I) = \Omega(I) \quad \dot{I} = 0$$

Those can be solved giving the solution

$$z = (\theta, I) = (\theta_0 + \Omega(I_0)t, I_0)$$

meaning the the angles move along the invariant torus $I = I_0$ with fixed frequency vector Ω [3]. Systems with ≥ 2 degrees of freedom cannot always be reduced to such form, giving rise to chaos. As examples, the 2-body problem is integrable but the N -body, $N > 2$, problem is nonintegrable.

If a system has the form

$$H(\theta, I) = H_0(I) + \varepsilon H'(\theta, I) \quad (1.10)$$

and is integrable at $\varepsilon = 0$, it still has a large set of invariant tori if $\varepsilon \ll 1$ [3]. This is the essence of Kolmogorov-Arnold-Moser (KAM) theory which is used to deal with persistence, under perturbation, of quasi-periodic motions[3]. Specifically the KAM theorem constitutes a condition for the preservation of regularity of motion and states:

THEOREM. *If the bounded motion of an integrable Hamiltonian H_0 is disturbed by a small perturbation $\varepsilon H'$ that makes the total Hamiltonian $H = H_0 + \varepsilon H'$ nonintegrable, and if*

- a. the perturbation is small*
- b. the frequencies w of H_0 are incommensurate*

then the motion remains confined on an N -torus except for a negligible set of initial conditions that result in a meandering trajectory in the energy surface.

That is when the perturbation is regarded as small the orbits will be stable, slightly altered, and will be bounded to the same region of phase space as the unperturbed ones.

One of the original motivations for KAM theory was to find bounded motions in the planetary $(N + 1)$ -body problem. Those systems can be seen as a perturbation of N decoupled two-body systems (star-planet). Essentially if masses, eccentricities, and inclinations are small enough (alternatively the planetary system lies in the neighborhood of circular and coplanar Keplerian orbits) there is subset of phase space leading to quasiperiodic motions, in which the semimajor axis remain close to original value, while eccentricities, and inclinations remain small[4].

1.3. CHAOS

Chaos, as observed in dynamical systems, is a phenomenon characterized by intricate, unpredictable, and aperiodic behaviors. It manifests within systems that exhibit nonlinearity resulting in a cascade of complex, seemingly random trajectories over time.

Its roots can be traced to the early 20th century. It was Lorenz in the 1960s that popularized chaos by his revelation of sensitive dependence on initial conditions that is epitomized by the metaphorical “butterfly effect”. Hamiltonian systems, such as exoplanet systems that this work examines, constitute dynamical systems and exhibit chaos. Specifically those are systems that have both regular (or ordered) and chaotic orbits in phase space.

There’s no universally accepted definition of chaos. A commonly used one formulated by R. L. Devaney. We start by defining the essential properties.

DEFINITION 1.1. *The $f: X \rightarrow X$ is sensitive dependent to initial conditions if*

$$\exists \delta > 0: \forall x \in X \forall \partial x \exists y \in \partial x \wedge n \geq 0: \|f^n(x) - f^n(y)\| > \delta$$

DEFINITION 1.2. *The $f: X \rightarrow X$ is topologically transitive if*

$$\forall U, V \subset X \exists k > 0: f^k(U) \cap V \neq \emptyset$$

DEFINITION 1.3. *The $f: X \rightarrow X$ has dense periodic orbits in X if*

$$\forall x \in X \exists \delta > 0 \wedge y \in \gamma(t; y): \|x - y\| < \delta$$

Intuitively, sensitive dependence to initial conditions exists if there are points arbitrarily close to x which eventually separate from x by at least distance δ under iteration, is topologically transitive if all points eventually move under iteration from one arbitrarily small neighborhood to any other, and has dense periodic orbits if every point is arbitrarily close to a periodic orbit.

Then the chaos definition according to Devaney states[5]:

DEFINITION 1.4. *Let X be a set and $f: X \rightarrow X$ a map on this set. Then f is chaotic on X if*

- i. f is sensitive to initial conditions*
- ii. f is topologically transitive*
- iii. f has dense periodic orbits in X*

This chaos definition gives chaos three components: unpredictability, non-partitioning into non-interacting subsystems, and regularity. For continuous maps it can be proved that the last two properties imply the first[6]. An also common weaker (as in having less properties) definition is utilizing only the first two properties.

Chaos detection techniques are split between two overarching categories: those based on visualization of orbits, such as Poincaré surface of section (also referred to as Poincaré section or Poincaré map), and those based on numerical analysis of orbits. Subcategory of the later are indicators based on the evolution of deviation vectors for a given orbit. It is those indicators that we will be examining.

1.4. NUMERICAL INTEGRATION METHODS

Differential equations, such as those describing the N -body problem, cannot be solved analytically in the general case. An alternative method is solving them numerically. There're few schemes but here we only present in depth the Bulirsch-Stoer, which is what we'll use in our numerical integration, and briefly the symplectic schemes that are often used in studies related to stability of dynamical systems.

1.4.1. Bulirsch-Stoer

The Bulirsch-Stoer method combines few ideas[7][8]; Richardson's extrapolation, polynomial extrapolation (or rational function extrapolation), and modified midpoint method.

Richardson's extrapolation considers the final answer of a numerical calculation as being an analytic function $f(h)$ of stepsize h . Then this function is probed by performing the calculation with various values h . When enough is known about the function, it's fit to some analytic form and then is evaluated at $h=0$. For the fit either a rational function or polynomial extrapolation is used. Finally, we have to use a method of which the error function is strictly even, allowing the fit function to be in terms h^2 . Such method is the modified midpoint.

The “modified” midpoint method takes n small steps of size h to cover the interval $t_0 \rightarrow t_0 + \tau$ (thus $h = \tau/n$). Then, considering \tilde{y} the mid approximations,

$$\begin{aligned} \tilde{y}_0 &= \tilde{y}(t_0) \\ \tilde{y}_1 &= \tilde{y}(t_1) = \tilde{y}_0 + h f(t_0, \tilde{y}_0) \\ \tilde{y}_{i+1} &= \tilde{y}(t_{i+1}) = \tilde{y}_{i-1} + h f(t_i, \tilde{y}_i) \quad t_i = t_0 + i h, i \in [1, n-1] \\ y(t_0 + \tau) &\approx \frac{1}{2} [\tilde{y}_n + \tilde{y}_{n-1} + h f(t_0 + \tau, \tilde{y}_n)] \end{aligned} \quad (1.11)$$

Its error series consists of only the even powers of h

$$y(t_0 + \tau) - y(t_0) = \sum k_i h^{2i}$$

The polynomial extrapolation is done taking two estimates for $y(t_0 + \tau)$ using n and $2n$ steps

$$y(t_0 + \tau) = \frac{4y_{2n} - y_n}{3}$$

This estimate is 4th order accurate, same as 4th order Runge-Kutta. If $Y_n^{(k)}$ represents the k -th order estimate then

$$Y_j^{(k+1)} = Y_j^{(k)} + \frac{Y_j^{(k)} - Y_{j-1}^{(k)}}{(n_j/n_{j-k})^2 - 1} \quad (1.12)$$

A B-S. method step covers $t_0 \rightarrow t_0 + \tau$ with n substeps of modified midpoint method which steps are then extrapolated to zero stepsize. The sequence of attempts to cover τ is made with increasing values of n , the number of substeps. The originally proposed sequence of n was $n_{j>3} = 2n_{j>3} - 2 = \{2, 4, 6, 8, 12, \dots\}$. A more performant sequence of n is $n_j = 2j = \{2, 4, 6, \dots\}$. After each n_j we extrapolate and obtain an error estimate. If satisfactory we go to next step.

1.4.2. Symplectic

A subcategory of geometric integrators; integrators preserving exactly some of the geometric properties of the phase-space flow. Assume the Hamilton function H is the sum of two separable parts, $T(p)$ and $V(q)$. Ignoring the second part

$$q' = q \quad p' = p - \tau \partial_q V \quad (1.13)$$

and ignoring the first part

$$p' = p \quad q' = q + \tau \partial_p V \quad (1.14)$$

By defining the operator $D_S = \{\cdot, S\}$ where $\{\cdot, \cdot\}$ the (antisymmetric) Poisson bracket, the equations of motion are written and solved as

$$\dot{\mathbf{z}} = \{\mathbf{z}, H\} = D_H \mathbf{z} \Rightarrow \mathbf{z} = e^{\tau D_H} \mathbf{z}_0 \quad (1.15)$$

Let $A = D_T$ and $B = D_V$ be the integrable parts of the Hamiltonian, and $D_H = D_T + D_V$ the sum of them. Then, the exact time evolution with step τ is given

$$\mathbf{z}(t + \tau) = e^{\tau D_H} \mathbf{z} = e^{\tau(A+B)} \mathbf{z} \quad (1.16)$$

The operator can be approached by an integrator of k steps. The two elementary algebraic maps are

$$e^{c_i \tau A} = \{q' = q + c_1 \tau p \quad p' = p\} \quad (1.17)$$

and

$$e^{d_i \tau B} = \{q' = q \quad p' = p - d_i \tau \partial_q V(q)\} \quad (1.18)$$

These maps give the exact solution for the canonical equations generative of the functions $\tilde{H} = H + O(\tau^2)$. The integrator preserves the energy of this new function but not the old although it bounds the energy error for H to $O(\tau^2)$.

The previous forms the basis for what is referred to as explicit method or $T + V$ algorithm. Higher-order integrators of that type are detailed in [9]. Taking advantage of the analytical solution in the unperturbed Keplerian problem, the mixed-variable integrators were developed which are efficient yet retain symplectic advantages. In brief, the Hamiltonian is split such that star-planet and intra-planetary interactions are separated. Then the star-planet part is evolved analytically.

1.5. SHOWCASING AN EXAMPLE SYSTEM

Consider the $d = 2$ mechanical system with unity masses

$$H = \frac{1}{2}(p_x^2 + p_y^2) + V(x, y)$$

in potential

$$V(x, y) = \frac{1}{2}(x^2 + y^2) + \left(x^2 y - \frac{1}{3}y^3\right)$$

This represents the Hénon–Heiles potential for $\lambda = 1$, the commonly taken value in classical chaos studies. The potential can be considered as the composition of two harmonic oscillators coupled with perturbation terms $x^2 y - y^3/3$. Setting λ leaves only one free parameter of the system, $H = h$ itself representing the energy of the system. Hénon–Heiles is a simple, yet providing complex motions, systems commonly used in chaos studies.

The Hamilton equations can be easily computed by hand and be found to assume the form

$$\begin{aligned} \dot{x} &= p_x & \dot{p}_x &= -x - 2xy \\ \dot{y} &= p_y & \dot{p}_y &= -y - (x^2 - y^2) \end{aligned}$$

Alternatively using the Maxima computer algebra system:

```
(%i1) V1: 1/2*(x^2+y^2) + x^2*y-y^3/3
```

```
(%o1) -y^3/3 + (y^2+x^2)/2 + x^2*y
```

```
(%i2) H1: 1/2*(p[x]^2+p[y]^2) + V1
```

```
(%o2) (p_y^2+p_x^2)/2 - y^3/3 + (y^2+x^2)/2 + x^2*y
```

```
(%i3) q1: [x, y]$
```

```
(%i4) p1: [p[x], p[y]]$
```

```
(%i5) qdot1: map(lambda([v], diff(H1, v)), p1)
```

```
(%o5) [p_x, p_y]
```

```
(%i6) pdot1: map(lambda([v], -diff(H1, v)), q1)
```

```
(%o6) [-2*x*y - x, y^2 - y - x^2]
```


Like other such systems, Maxima provides a routine for numerically integrating ODEs and the utilized integrator is a 4th order Runge-Kutta method. We choose the following initial conditions:

Type	h	x_0	y_0	\dot{y}_0
regular	0.125	0	0.1	0
chaotic	0.125	0	-0.25	0

Table 1.1.

Then first finding $\dot{x}_0 = p_{x;0}$ from Hamiltonian, we can solve the initial value problem and plot the trajectory for each of the initial conditions.

```
(%i7) solve(H1 = 0.125, p[x]), x=0, p[y]=0, y=0.1
```

```
rat: replaced -0.1203333333333333 by -361/3000 = -0.1203333333333333
```

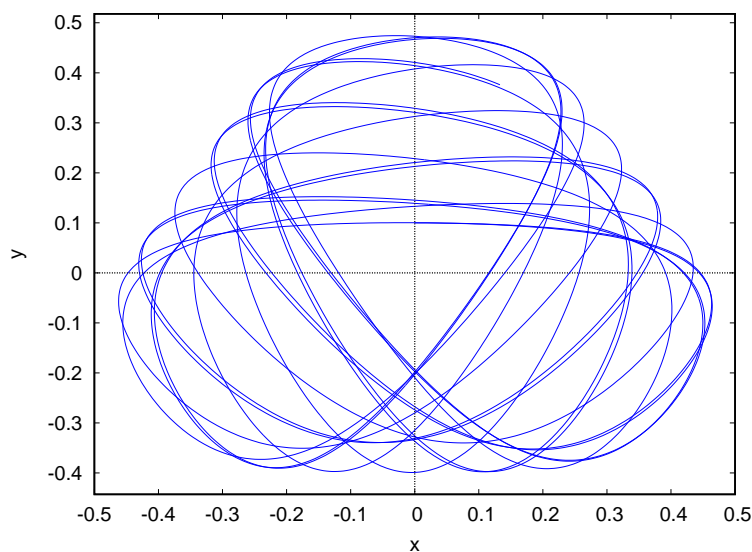
```
(%o7) [p0 = -19/(10*sqrt(15)), p0 = 19/(10*sqrt(15))]
```

```
(%i8) float(%)
```

```
(%o8) [p0 = -0.490577890519606, p0 = 0.490577890519606]
```

```
(%i9) solr: rk(
  [px,py,-2*x*y-x,y^2-y-x^2],
  [x,y,px,py],
  [0,0.1,0.490577890519606,0],
  [t, 0, 100, 0.02])$
```

```
(%i10) tm_plot2d([discrete, makelist(
  [p[2], p[3]], p, solr)], [xlabel, "x"], [ylabel, "y"])$
```



```
(%i11) solve(H1 = 0.125, p[x]), x=0, p[y]=0, y=-0.25
```

```
rat: replaced -0.08854166666666666 by -17/192 = -0.08854166666666667
```

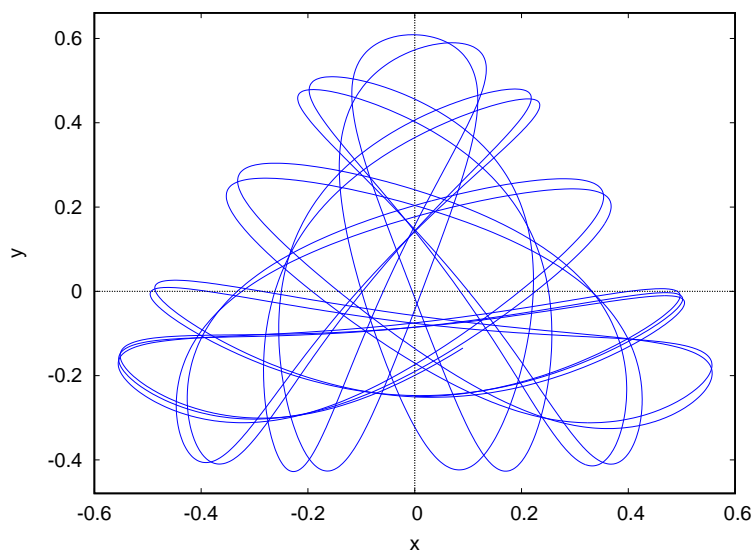
```
(%o11)  $\left[ p_0 = -\frac{\sqrt{17}}{4\sqrt{6}}, p_0 = \frac{\sqrt{17}}{4\sqrt{6}} \right]$ 
```

```
(%i12) float(%)
```

```
(%o12)  $[p_0 = -0.4208127057650867, p_0 = 0.4208127057650867]$ 
```

```
(%i13) solir: rk(
    [px,py,-2*x*y-x,y^2-y-x^2],
    [x,y,px,py],
    [0,-0.25,0.4208127057650867,0],
    [t, 0, 100, 0.02])$
```

```
(%i14) tm_plot2d([discrete, makelist(
    [p[2], p[3]], p, solir)], [xlabel, "x"], [ylabel, "y"])$
```

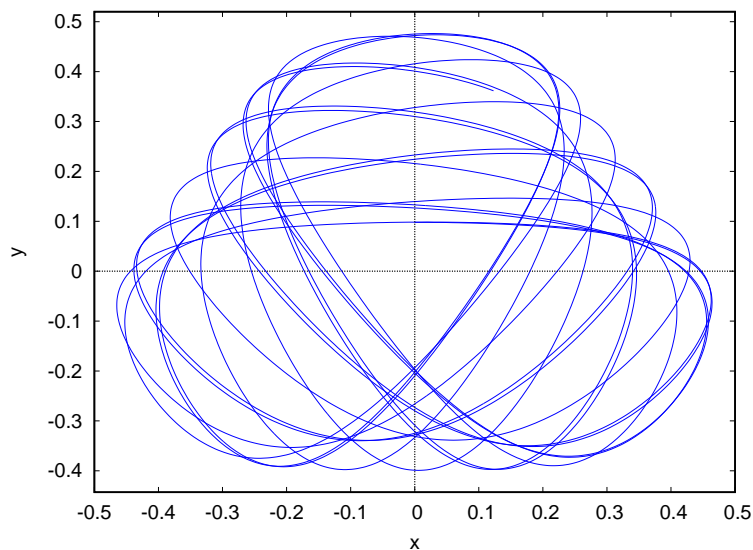


Notice how the dynamics differ and in the case of chaotic orbit the movement appears aperiodic and random. Nevertheless, as expected from KAM theorem due to perturbation being small, the motion is bounded to the same region as the regular orbit and is similar in shape.

Let's try again by introducing a small displacement in the initial conditions.

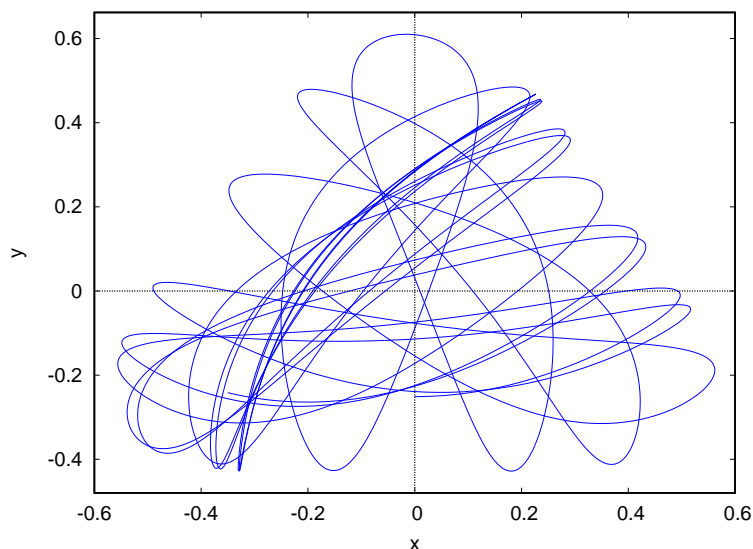
```
(%i15) solr2: rk(
    [px,py,-2*x*y-x,y^2-y-x^2],
    [x,y,px,py],
    [0,0.1-0.002,0.490577890519606,0],
    [t, 0, 100, 0.02])$
```

```
(%i16) tm_plot2d([discrete, makelist(
    [p[2], p[3]], p, solr2)], [xlabel, "x"], [ylabel, "y"])$
```



```
(%i17) solir2: rk(
    [px,py,-2*x*y-x,y^2-y-x^2],
    [x,y,px,py],
    [0,-0.25-0.001,0.4208127057650867,0],
    [t, 0, 100, 0.02])$
```

```
(%i18) tm_plot2d([discrete, makelist(
    [p[2], p[3]], p, solir2)], [xlabel, "x"], [ylabel, "y"])$
```

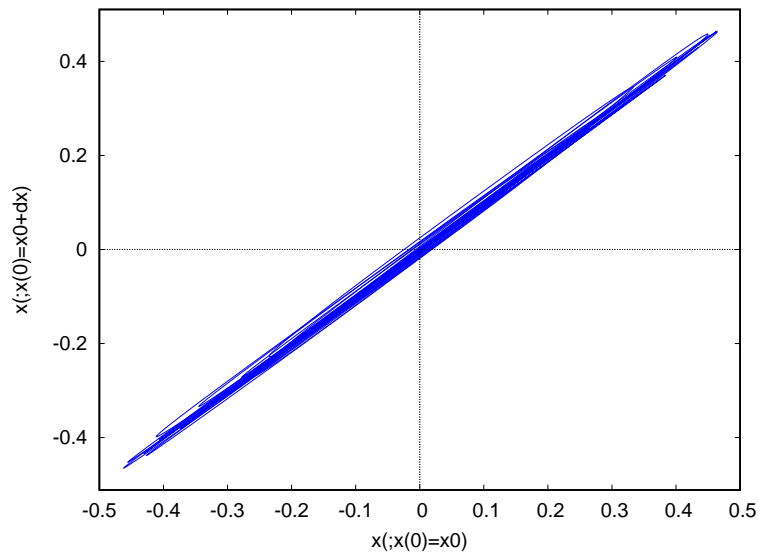


We then plot the evolution portraits for $x(;x(0) = x_0)$ and $x(;x(0) = x_0 + dx)$ for the regular and irregular orbit.

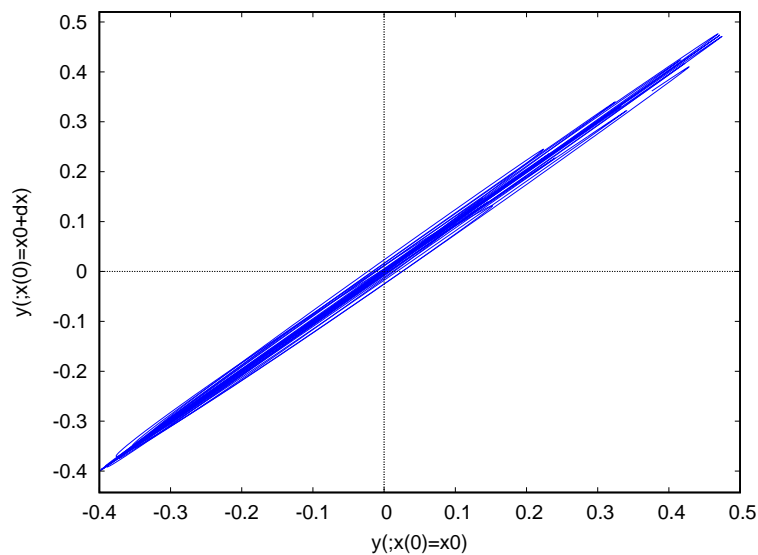
```
(%i19) zip(lst1, lst2) := makelist([lst1[i],lst2[i]],i,1,length(lst1))$
```

```
(%i20) makezip(d, lst1, lst2) :=  
      zip(makelist(p[d],p,lst1),makelist(p[d],p,lst2))$
```

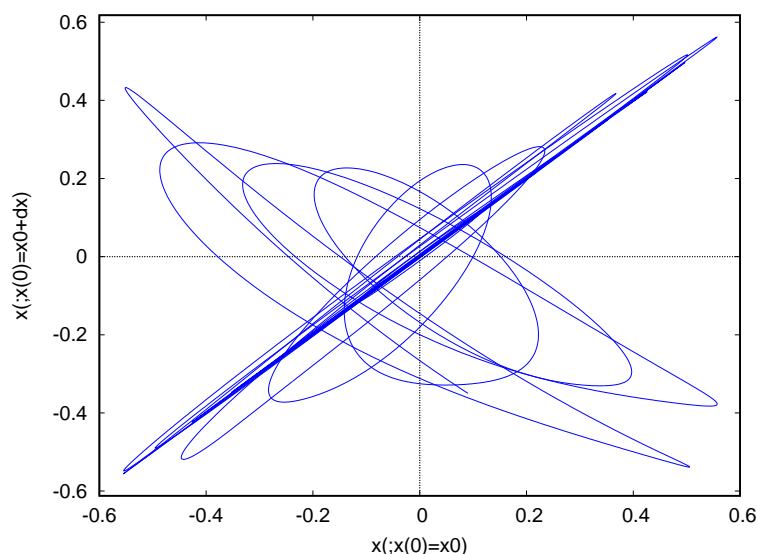
```
(%i21) tm_plot2d([discrete, makezip(2,solr,solr2)],  
      [xlabel, "x(;x(0)=x0)", [ylabel, "x(;x(0)=x0+dx)"]])$
```



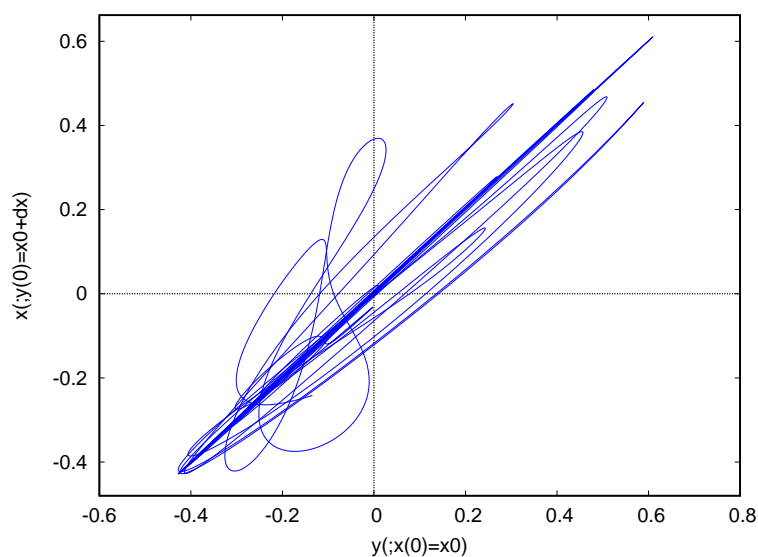
```
(%i22) tm_plot2d([discrete, makezip(3,solr,solr2)],  
      [xlabel, "y(;x(0)=x0)", [ylabel, "y(;x(0)=x0+dx)"]])$
```



```
(%i23) tm_plot2d([discrete, makezip(2,solir,solir2)],
  [xlabel, "x(;x(0)=x0)", [ylabel, "x(;x(0)=x0+dx)"]])$
```



```
(%i24) tm_plot2d([discrete, makezip(3,solir,solir2)],
  [xlabel, "y(;x(0)=x0)", [ylabel, "x(;y(0)=x0+dx)"]])$
```



Notice that in case of regular orbit, the disturbed (or perturbed) orbit closely follows the original. For the chaotic this only happens at the beginning and then quickly diverges from the original. This is the essence of chaos and its sensitive dependence on initial conditions when it exists.

Although Maxima and other symbolic algebra systems can numerically integrate such equations, for the times required for dynamical studies they're very slow to provide result in case of more complex systems such as the N -body problem. Rather using such packages, high performant code is better fit for those. Based on theory presented in this chapter we'll be using an in-house built B.-S. integrator to perform the numerical integrations of the final chapter.

CHAPTER 2

CELESTIAL MECHANICS

The branch of astronomy dealing with the motions of celestial bodies, usually but not necessary utilizing principles of classical mechanics and oftentimes restricted to gravitation, has come to be called celestial mechanics. Being a centuries old science means only a brief background can be provided which for our work is enough.

At the heart of classical celestial mechanics lies the application of Newtonian mechanics and gravitational theory to celestial objects. Early luminaries such as J. Kepler, I. Newton, and P.-S. Laplace established the fundamental principles that underpin the field, including Kepler's laws of planetary motion and Newton's law of universal gravitation. These principles enabled astronomers to predict the orbits and positions of celestial bodies with remarkable accuracy, altering our understanding of the cosmos.

Celestial mechanics also delves into the study of gravitational perturbations, where the gravitational interactions among celestial bodies lead to subtle but critical alterations in their orbits.

2.1. ORBITS

The general parameters (derived from mechanics) characterizing orbital motions are

- Position (\mathbf{r}): the vector of the orbiting body's position relative to the inertial frame and point of origin.
- Velocity (\mathbf{v}): the vector of the orbiting body's velocity relative to the inertial frame and point of origin.
- Specific angular momentum ($\mathbf{h} = \mathbf{r} \times \mathbf{v}$): the orbiting body's angular momentum divided by its mass.
- Specific energy (ϵ): the total energy of the system divided by the reduced mass.
- Period (P): the time it takes for the orbiting body to make a complete closed trajectory around the main body.
- Gravitational parameter (μ): simply defined as $\mu = G(m_0 + m) \approx Gm_0$

The, also called orbital state, vectors of position r and velocity v uniquely determine the trajectory of an orbiting body and are defined with respect to a reference frame. The orbit coinciding with the current orbital state vectors is called osculating orbit.

As orbits follow conic sections it's more convenient characterizing the motions by quantities describing the geometrical properties of the orbit and the position on it. Orbital elements are the parameters that uniquely identify a specific orbit and the instantaneous position of the body on it. In absence of perturbation all but the one characterizing the position are time independent. In the perturbed case vary non-linearly and in real astronomical orbits the osculating elements can evolve very quickly. The orbital elements are:

- Semimajor axis (a): the sum of the periapsis and apoapsis distances divided by two.
- Eccentricity (e): describes how much elongated is the ellipse compared to a circle.
- Inclination (i): the vertical tilt of the ellipse with respect to the reference plane; it's measured at the ascending node where the orbit passes upward through the reference plane.

- Longitude of the ascending node (Ω): horizontal orientation of the ascending node.
- Argument of periaapsis (ω): orientation of the ellipse in the orbital plane; it's measure from the ascending node to the periaapsis.
- True anomaly ($\nu = \nu(t)$): position of the orbiting body along the ellipse.

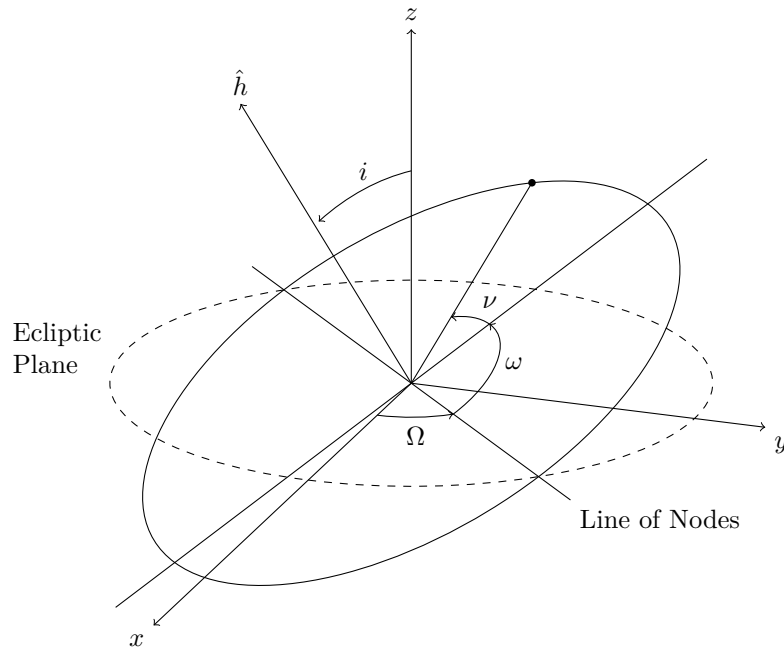


Figure 2.1. Orbital elements shown schematically. The Euler-like angles i , Ω , ω describe the orientation of the orbit relative to the ecliptic plane. The true anomaly specifies the position of the orbiting body.

The first two parameters specify the shape of the ellipse, the next three the orientation, corresponding to the three Euler angles, and the last one the position of the body on the orbit. Besides those parameters the following are introduced:

- Eccentric anomaly ($E = E(t)$): the angle subtended at the center of the ellipse by the projection of the position on the circle with radius a and tangent to the ellipse at pericenter and apocentre.
- Mean anomaly ($M = M(t)$): the angular distance from the pericenter at arbitrary time. The mean and eccentric anomaly are connected via the Kepler's equation $M = E - e \sin E$.
- Longitude of pericenter (ϖ): defined $\varpi = \Omega + \omega$.
- Mean longitude ($\lambda = \lambda(t)$): defined $\lambda = \varpi + M$.

Thus the tuple $(a, e, i, \Omega, \omega, \nu$ or E or $M)$ gives the instantaneous position of the orbiting body and is equivalent to the tuple (\mathbf{r}, \mathbf{v}) , $\mathbf{r} = (x, y, z)$, $\mathbf{v} = \dot{\mathbf{r}} = (\dot{x}, \dot{y}, \dot{z})$.

2.2. EQUATIONS OF MOTION

Celestial bodies are assumed to be point masses (planetary systems) or rigid or deformable bodies (satellite geodesy and Earth rotation)[10]. We'll only concentrate to first that is a system of point masses and only considering gravitational forces. Some basic concepts such as inertial frames are assumed known.

Let's start with a body, viewed as a particle, in orbit around a more massive one. The kinetic energy of the orbiting body is given

$$T(\mathbf{p}) = \frac{p^2}{2m} \quad (2.1)$$

and the gravitation potential energy of a particle in orbit is obtained

$$V(\mathbf{q}) = -\frac{m\mu}{q} \Rightarrow V(\mathbf{q}) = -G\frac{mm_0}{q} \quad (2.2)$$

where G is the gravitational constant, μ is the gravitational parameter depending on the mass of the massive body, and $\mathbf{q} = \mathbf{r}, \mathbf{p} = m\dot{\mathbf{r}}$. The Hamiltonian governing the motion of the orbiting body then is

$$H = \frac{p^2}{2m} - \frac{m\mu}{q} \Rightarrow H = \frac{p^2}{2m} - G\frac{mm_0}{q} \quad (2.3)$$

and the Hamilton equations become

$$\dot{\mathbf{q}} = \mathbf{p} \quad \dot{\mathbf{p}} = -m\mu \mathbf{q}/q^3 \quad (2.4)$$

Those are the equations of motion of the body under the gravitational influence of the massive one.

2.3. *N*-BODY PROBLEM

As *N*-body is called the problem of predicting the individual motions of a gravitationally interacting group of objects. The case of planets or/and stars in dynamical systems theory represents a small-*N* system.

The potential field for a body i under the influence of the $N - 1$ other bodies is

$$V_i(\mathbf{q}) = -G \sum_{i=1, j \neq i}^N \frac{m_i m_j}{q_{ij}} \quad (2.5)$$

The Hamiltonian of the system is then written as

$$H = T(\mathbf{p}) + V(\mathbf{q}) = \sum_{i=1}^N \frac{p_i^2}{2m_i} - G \sum_{i=1, j > i}^N \frac{m_i m_j}{q_{ij}} \quad (2.6)$$

where G is the gravitational constant and $q_{ij} = \|\mathbf{q}_{ij}\| = \|\mathbf{q}_i - \mathbf{q}_j\|$. Then the Hamilton equations take the form

$$\dot{\mathbf{q}}_i = \mathbf{p}_i \quad \dot{\mathbf{p}}_i = -G \sum_{j=1, j \neq i}^N \frac{m_i m_j}{q_{ij}^3} \mathbf{q}_{ij} \quad (2.7)$$

Similar to free particle, those are the equations of motion of body i under the gravitational influence of the other bodies. Those are $6N$ equations in total. There're scalar functions of positions and velocities that are known to be time-independent. Those are the *first integrals* of the system. The energy and the angular momentum are such quantities as

$$\dot{H} = 0 \quad \dot{\mathbf{L}} = \frac{d}{dt} \sum_i \mathbf{q}_i \times \mathbf{p}_i = 0 \quad (2.8)$$

Extending for the later

$$\sum_{i=1}^N m_i \mathbf{q}_i \times \ddot{\mathbf{q}}_i = G \sum_{i, j=1, j \neq i}^N \frac{m_i m_j}{q_{ij}^3} \mathbf{q}_i \times \mathbf{q}_{ij} = 0 \Rightarrow \sum_{i=1}^N m_i \mathbf{q}_i \times \dot{\mathbf{q}}_i = C \quad (2.9)$$

The relationship states the total angular momentum of the system remains constant. The previous relationship can be rewritten in coordinates to reference frame as

$$\begin{aligned} L_x &= \sum_{i=1}^N m_i (y_i \dot{z}_i - z_i \dot{y}_i) = c \\ L_y &= \sum_{i=1}^N m_i (z_i \dot{x}_i - x_i \dot{z}_i) = c \\ L_z &= \sum_{i=1}^N m_i (x_i \dot{y}_i - y_i \dot{x}_i) = c \end{aligned} \quad (2.10)$$

The former can also be found via the equations of motion (Newtonian approach)

$$\sum_{i=1}^N m_i \dot{\mathbf{q}}_i \ddot{\mathbf{q}}_i = G \sum_{i,j=1, j \neq i}^N \frac{m_i m_j}{q_{ij}^3} \dot{\mathbf{q}}_i \mathbf{q}_{ij} \Rightarrow \frac{1}{2} \sum_{i=1}^N m_i \dot{\mathbf{q}}_i \dot{\mathbf{q}}_i - \frac{1}{2} \sum_{i,j=1, j \neq i}^N \frac{m_i m_j}{q_{ij}} = E \quad (2.11)$$

which can be rewritten

$$E = T + U \quad (2.12)$$

where

$$T = \frac{1}{2} \sum_{i=1}^N m_i \dot{q}_i^2 = \sum_{i=1}^N \frac{p_i^2}{2m_i} \quad U = -\frac{1}{2} \sum_{i,j=1, j \neq i}^N \frac{m_i m_j}{q_{ij}} \quad (2.13)$$

The position and momentum of center of mass is found

$$(\mathbf{q}_{\text{CM}}, \mathbf{p}_{\text{CM}}) = \frac{1}{m_{\text{tot}}} \sum_{i=1}^N m_i (\mathbf{q}_i, \mathbf{p}_i) \quad (2.14)$$

where $m_{\text{tot}} = \sum m_i$ the total mass of the system.

By summing $\dot{\mathbf{p}}_i$ and integrating twice

$$\sum_{i=1}^N m_i \ddot{\mathbf{q}}_i = 0 \Rightarrow \sum_{i=1}^N m_i \dot{\mathbf{q}}_i = \mathbf{c}_1 \Rightarrow \sum_{i=1}^N m_i \mathbf{q}_i = \mathbf{c}_1 t + \mathbf{c}_2 \quad (2.15)$$

The $\mathbf{c}_1, \mathbf{c}_2$ rewritten in coordinates to reference frame provide the last integrals of motion. The relationships state that total momentum is conserved and that the center of mass moves in space with constant velocity and hence can be considered as stable to the system's inertial frame.

For computational purposes, the conservation of energy and angular momentums introduce an accuracy indicator to the utilized integration scheme, whereas the stability of the center of mass can be utilized to reduce the integrated equation set from that of N bodies to $N - 1$ as the position and velocity of the N th body can be deduced from the center of mass after all other bodies have moved.

2.4. PLANETARY PROBLEM

In a planetary system we have few small objects, the planets, orbiting a large one (also called the primary body), the host star. Based on that we assume that $n = N + 1$. All objects are assumed to be of constant mass. We can rewrite the equations of motions as

$$\ddot{\mathbf{r}} = -G \sum_{j=1, j \neq i}^N \frac{m_j}{r_{ij}^3} \mathbf{r}_{ij} \quad (2.16)$$

If mass m_0 dominates all other masses it makes sense to rearrange the equation to describe the motion relative to the position of mass m_0 . We introduce the vectors

$$\mathbf{r}_i = \mathbf{x}_i - \mathbf{x}_0 \quad (2.17)$$

called the heliocentric position vectors. The equations of motion in the inertial system can be converted to corresponding equations in heliocentric frame subtracting the equation for mass m_0 from the equation for mass $m_{i>0}$. We obtain

$$\ddot{\mathbf{r}}_i = \ddot{\mathbf{x}}_i - \ddot{\mathbf{x}}_0 = -G \sum_{j=1, j \neq i}^n \frac{m_j}{r_{ij}^3} \mathbf{r}_{ij} - G \sum_{j=1}^n \frac{m_j}{r_j^3} \mathbf{r}_j \quad (2.18)$$

It can be rewritten in the form

$$\ddot{\mathbf{r}}_i = -G(m_0 + m_i) \frac{\mathbf{r}_i}{r_i^3} - \sum_{j=1, j \neq i}^n m_j \left(\frac{\mathbf{r}_{ij}}{r_{ij}^3} - \frac{\mathbf{r}_j}{r_j^3} \right) \quad (2.19)$$

The Hamiltonian of the system is

$$H = T(\mathbf{p}) + V(\mathbf{q}) = \frac{p_0^2}{2m_0} + \sum_{i=1}^n \left(\frac{p_i^2}{2m_i} - G \frac{m_0 m_i}{r_{0i}} \right) - G \sum_{i=1, j>i}^n \frac{m_i m_j}{r_{ij}} \quad (2.20)$$

2.5. SHOWCASING IN 3-PLANET SYSTEM

As a specific example to previous, we are showcasing the 3-planet system that we'll numerical study in the final section. The equations are extracted using the Maxima computer algebra system.

```
(%i1) Hnb(n) := sum(p[i]^2/(2*m[i]), i, 0, n) -
      G*sum(sum(m[i]*m[j]/(q[j]-q[i]), j, i+1, n), i, 0, n)$
```

```
(%i2) Hnb(n)
```

$$(%o2) \frac{\sum_{i=0}^n \frac{p_i^2}{m_i}}{2} - G \sum_{i=0}^n m_i \sum_{j=i+1}^n \frac{m_j}{q_j - q_i}$$

```
(%i3) H3 : Hnb(3)
```

$$(%o3) - \left(\frac{m_2 m_3}{q_3 - q_2} + \frac{m_1 m_3}{q_3 - q_1} + \frac{m_0 m_3}{q_3 - q_0} + \frac{m_1 m_2}{q_2 - q_1} + \frac{m_0 m_2}{q_2 - q_0} + \frac{m_0 m_1}{q_1 - q_0} \right) G + \frac{p_3^2}{2 m_3} + \frac{p_2^2}{2 m_2} + \frac{p_1^2}{2 m_1} + \frac{p_0^2}{2 m_0}$$

```
(%i4) map(lambda([v], declare(v,constant)), cons(G,makelist(m[i],i,0,3)))$
```

```
(%i5) q3 : makelist(q[i],i,0,3)$
```

```
(%i6) p3 : makelist(p[i],i,0,3)$
```

```
(%i7) qdot3 : map(lambda([v], diff(H3, v)), p3)
```

$$(%o7) \left[\frac{p_0}{m_0}, \frac{p_1}{m_1}, \frac{p_2}{m_2}, \frac{p_3}{m_3} \right]$$

```
(%i8) pdot3 : map(lambda([v], -diff(H3, v)), q3)
```

$$\begin{aligned}
 (%o8) \left[\left(\frac{m_0 m_3}{(q_3 - q_0)^2} + \frac{m_0 m_2}{(q_2 - q_0)^2} + \frac{m_0 m_1}{(q_1 - q_0)^2} \right) G, \left(\frac{m_1 m_3}{(q_3 - q_1)^2} + \frac{m_1 m_2}{(q_2 - q_1)^2} - \right. \right. \\
 \left. \frac{m_0 m_1}{(q_1 - q_0)^2} \right) G, \left(\frac{m_2 m_3}{(q_3 - q_2)^2} - \frac{m_1 m_2}{(q_2 - q_1)^2} - \frac{m_0 m_2}{(q_2 - q_0)^2} \right) G, \left(-\frac{m_2 m_3}{(q_3 - q_2)^2} - \frac{m_1 m_3}{(q_3 - q_1)^2} - \right. \\
 \left. \frac{m_0 m_3}{(q_3 - q_0)^2} \right) G \Big]
 \end{aligned}$$

Note that differentiation was done considering values as scalars. But actually each component after requires the unit vector \mathbf{q}_{ij}/q_{ij} resulting in the theoretical written \mathbf{q}_{ij}/q_{ij}^3 values.

CHAPTER 3

VARIATIONAL EQUATIONS (VEQS)

Variational equations constitute a foundational concept within the realm of dynamical systems theory, offering a powerful mathematical framework for probing the sensitivity and stability of evolving systems. These equations are a key instrument in assessing how small perturbations or variations in a system's initial conditions or parameters can lead to significant alterations in its trajectory or behavior over time. They exist for all initial value problems[11] and most often appear in[11] stability studies for specific solutions of differential equations, parameter estimation theory, and error propagation theory in numerical integration.

3.1. VEQS OF DYNAMICAL SYSTEMS

We want to derive the variational equations associated with the general initial value problem

$$\begin{aligned} \mathbf{x}^{(n)} &= \mathbf{f}(t; \mathbf{x}, \dot{\mathbf{x}}, \ddot{\mathbf{x}}, \dots, \mathbf{x}^{(n-1)}, \tilde{p}_1, \tilde{p}_2, \dots, \tilde{p}_m) \\ \mathbf{x}^{(i)}(t_0) &= \mathbf{x}_0^{(i)}, \quad i = 0, 1, \dots, n-1 \end{aligned} \quad (3.1)$$

The initial value problem is referred to as the *primary equations* system. The dynamical parameters \tilde{p}_i are included so the impact of changing one or more of them can be studied. The orbital elements of the planets and even masses if those aren't considered constant are such examples of dynamical parameters.

The partial derivative of the solution vector is designated

$$\mathbf{w}(t) = \frac{\partial \mathbf{x}}{\partial p} \quad (3.2)$$

By taking the partial derivatives with respect to the components of the solution vector and its first $n-1$ derivatives, then the partial derivatives of these components with respect to parameter p , the previous is a particular solution of the system

$$\mathbf{w}^{(n)}(t) = \sum_{i=0}^{n-1} \mathbf{A}_i(t) \mathbf{w}^{(i)}(t) + \mathbf{f}_p(t) \quad (3.3)$$

where the components of the square matrices of dimension $d \times d$

$$A_{i,jk}(t) = \frac{\partial f_j}{\partial x_k^{(i)}} \quad (3.4)$$

are the elements of the Jacobian of vector $\mathbf{f}(\dots)$. This differential equation system is called the system of variational equations for parameter p of the original system (the primary equations). If the partial derivatives are with respect only to the components then the system assumes the form

$$\mathbf{w}^{(n)}(t) = \sum_{i=0}^{n-1} \mathbf{A}_i(t) \mathbf{w}^{(i)}(t) \quad (3.5)$$

As initial conditions can take the tangent direction to the flow, that is

$$\mathbf{w}_0 = \frac{\dot{\mathbf{x}}}{\|\dot{\mathbf{x}}\|} \quad (3.6)$$

but depending on problem another set of initial conditions can be taken (or even preferred).

A benefit of integrating the system of variational equations along the primary system is the obtainment of information concerning its (first order) stability within the time interval of the integration.

3.2. VEQS OF HAMILTONIAN SYSTEMS

Let's consider an autonomous Hamiltonian system having a function

$$H(q_1, q_2, \dots, q_N, p_1, p_2, \dots, p_N) = h = \text{const.} \quad (3.7)$$

where the $q_i, p_i, i = 1, 2, \dots, N$ the generalized coordinates and conjugate momenta respectively. An orbit is defined by the vector

$$\mathbf{x}(t) = (q_1(t), q_2(t), \dots, q_N(t), p_1(t), p_2(t), \dots, p_N(t)) \quad (3.8)$$

where $x_i = q_i, x_{i+N} = p_i, i = 1, 2, \dots, N$.

The time evolution of the orbit is governed by the Hamilton's equations of motion

$$\dot{\mathbf{z}} = \mathbf{J} \cdot \nabla H =: \mathbf{J} \cdot \mathbf{D}_H \quad (3.9)$$

An initial deviation vector $\mathbf{w}(t_0) = \delta \mathbf{z}(t_0)$ from an orbit $\mathbf{z}(t)$ evolves in tangent space according to the equations

$$\dot{\mathbf{w}} = (\mathbf{J} \cdot \mathbf{D}_H^2(\mathbf{z}(t))) \cdot \mathbf{w} = \mathbf{A}(t) \cdot \mathbf{w} \quad (3.10)$$

with $\mathbf{D}_H^2(\mathbf{z}(t))$ is the Hessian matrix of Hamiltonian calculated on the reference orbit, i.e.,

$$\mathbf{D}_H^2(\mathbf{z}(t)) = \frac{\partial^2 H}{\partial z_i \partial z_j} \quad (3.11)$$

We now consider an autonomous mechanical system, that is one of which the Hamiltonian assumes the form

$$H = \sum_{i=1}^N \frac{p_i^2}{2m_i} + V(\mathbf{q}) \quad (3.12)$$

The Hamilton equations become

$$\dot{\mathbf{z}} = \begin{pmatrix} \dot{\mathbf{q}} \\ \dot{\mathbf{p}} \end{pmatrix} = \begin{pmatrix} \mathbf{p} \\ -\partial_{\mathbf{q}} V(\mathbf{q}) \end{pmatrix} \quad (3.13)$$

and the variational equations take the form

$$\dot{\mathbf{w}} = \begin{pmatrix} \delta \dot{\mathbf{q}} \\ \delta \dot{\mathbf{p}} \end{pmatrix} = \begin{pmatrix} \delta \mathbf{p} \\ -\mathbf{D}_V^2(\mathbf{q}(t)) \delta \mathbf{q} \end{pmatrix} \quad (3.14)$$

with $\mathbf{D}_V^2(\mathbf{q}(t))$ written

$$\mathbf{D}_V^2(\mathbf{q}(t)) = \frac{\partial^2 V(\mathbf{q})}{\partial q_j \partial q_k} \quad (3.15)$$

The tangent dynamics of the Hamiltonian is represent by the time-dependent Hamiltonian function

$$H_V(\delta \mathbf{q}, \delta \mathbf{p}; t) = \frac{1}{2} \sum_{i=1}^N \delta p_i^2 + \frac{1}{2} \sum_{j,k=1}^N \mathbf{D}_V^2(\mathbf{q}(t))_{jk} \delta q_j \delta q_k \quad (3.16)$$

which is called the *tangent dynamics Hamiltonian* (THD) and of which the equations of motion are exactly the variational equations[12].

The deviation vector of body i is, according to previous, given by

$$\dot{\mathbf{w}}_i = \begin{pmatrix} \delta \dot{\mathbf{q}}_i \\ \delta \dot{\mathbf{p}}_i \end{pmatrix} = \begin{pmatrix} \delta \mathbf{p}_i \\ -\mathbf{D}_V^2(\mathbf{q}_i(t))\delta \mathbf{q}_i \end{pmatrix} \quad (3.17)$$

For a $6N$ order system (motion in 3d space, such as the N -body problem), $\delta \mathbf{o}(t) = (\delta o_{ik})$, $\mathbf{q}_i = (q_{ik})$, $k = 1, 2, 3$, and[9]

$$\mathbf{D}_V^2(\mathbf{q}_i(t)) = \begin{pmatrix} \frac{\partial^2 V}{\partial q_{i1}^2} & \frac{\partial^2 V}{\partial q_{i1}\partial q_{i2}} & \frac{\partial^2 V}{\partial q_{i1}\partial q_{i3}} \\ \frac{\partial^2 V}{\partial q_{i1}\partial q_{i2}} & \frac{\partial^2 V}{\partial q_{i2}^2} & \frac{\partial^2 V}{\partial q_{i2}\partial q_{i3}} \\ \frac{\partial^2 V}{\partial q_{i1}\partial q_{i3}} & \frac{\partial^2 V}{\partial q_{i2}\partial q_{i3}} & \frac{\partial^2 V}{\partial q_{i3}^2} \end{pmatrix} \quad (3.18)$$

and thus

$$\mathbf{D}_V^2(\mathbf{q}_i(t))\delta \mathbf{q}_i = \begin{pmatrix} \frac{\partial^2 V}{\partial q_{i1}^2}\delta q_{i1} + \frac{\partial^2 V}{\partial q_{i1}\partial q_{i2}}\delta q_{i2} + \frac{\partial^2 V}{\partial q_{i1}\partial q_{i3}}\delta q_{i3} \\ \frac{\partial^2 V}{\partial q_{i1}\partial q_{i2}}\delta q_{i1} + \frac{\partial^2 V}{\partial q_{i2}^2}\delta q_{i2} + \frac{\partial^2 V}{\partial q_{i2}\partial q_{i3}}\delta q_{i3} \\ \frac{\partial^2 V}{\partial q_{i1}\partial q_{i3}}\delta q_{i1} + \frac{\partial^2 V}{\partial q_{i2}\partial q_{i3}}\delta q_{i2} + \frac{\partial^2 V}{\partial q_{i3}^2}\delta q_{i3} \end{pmatrix} \quad (3.19)$$

3.3. VEQS OF N -BODY PROBLEM

Let's consider an N -body system. We follow [13] which utilizes the same approach shown previously. Alternatively we could substitute the gravitational potential in the previous equations. The differential equations for the N -body problem are

$$\ddot{\mathbf{r}} = -G \sum_{j=1, j \neq i}^N \frac{m_j}{r_{ij}^3} \mathbf{r}_{ij} \quad (3.20)$$

or in component form

$$\dot{v}_{i,a} = -G \sum_{j=1, j \neq i}^N \frac{m_j}{r_{ij}^3} r_{ij,a} \quad (3.21)$$

Differentiating the equations with respect to $r_{j,b}$

$$\begin{aligned} \frac{\partial \dot{v}_{i,a}}{\partial r_{j,b}} &= \frac{\partial}{\partial r_{j,b}} \left(-G \sum_{k, k \neq i} \frac{m_k r_{ik,a}}{r_{ik}^3} \right) \\ &= -G \sum_{k, k \neq i} \frac{m_k (\delta_{ij} - \delta_{kj}) \delta_{ab}}{r_{ik}^3} + G \sum_{k, k \neq i} \frac{3m_k r_{ik,a} r_{ik,b}}{r_{ik}^5} \\ &= \begin{cases} G \sum_{k, k \neq i} \left(-\frac{m_k \delta_{ab}}{r_{ik}^3} + 3 \frac{m_k r_{ik,a} r_{ik,b}}{r_{ik}^5} \right) & \text{if } i = j \\ +G \frac{m_j \delta_{ab}}{r_{ij}^3} - G \frac{3m_j r_{ij,a} r_{ij,b}}{r_{ij}^5} & \text{if } i \neq j \end{cases} \end{aligned} \quad (3.22)$$

Those are of course the elements of the Hessian matrix of the potential. The interested reader can refer to [13] if they want to introduce varying masses in the system. The aforementioned reference also derives the 2nd-order N -body variational equations.

3.4. VEQS OF PLANETARY PROBLEM

For simplicity let's first consider the 2-body problem. According to the previous procedure, the corresponding variational equations are obtained by taking the partial derivative of the respective equations. The result is[11]

$$\ddot{\mathbf{w}} = -\frac{\mu}{r^3} \begin{pmatrix} 1 - 3\frac{r_1^2}{r^2} & -\frac{3r_1r_2}{r^2} & -\frac{3r_1r_3}{r^2} \\ -\frac{3r_1r_2}{r^2} & 1 - \frac{3r_2^2}{r^2} & -\frac{3r_2r_3}{r^2} \\ -\frac{3r_1r_3}{r^2} & -\frac{3r_2r_3}{r^2} & 1 - \frac{3r_3^2}{r^2} \end{pmatrix} \quad (3.23)$$

which can be rewritten with the more compact notation

$$\ddot{\mathbf{w}} = -\frac{\mu}{r^3} \left(\mathbf{E} - \frac{3}{r^2} \mathbf{r} \otimes \mathbf{r}^T \right) \mathbf{w} \quad (3.24)$$

where $\mathbf{r} \otimes \mathbf{r}^T$ is the Cartesian, or outer, product of the column array \mathbf{r} with its transpose \mathbf{r}^T . Similar to the differential equations of the 2-body problem, it's possible to derive closed solutions of the previous variational equations[11].

The differential equations of n -planet system can be written

$$\ddot{\mathbf{r}}_i = -G(m_0 + m_i) \frac{\mathbf{r}_i}{r_i^3} - \sum_{j=1, j \neq i}^n m_j \left(\frac{\mathbf{r}_{ij}}{r_{ij}^3} - \frac{\mathbf{r}_j}{r_j^3} \right) \quad (3.25)$$

The variational equations for the planetary system are obtained by taking the partial derivative of the primary equations. To simplify the resulting equations the auxiliary matrices \mathbf{C}_{ij} , \mathbf{C}_{i0} , \mathbf{A}_{ij} , \mathbf{A}_{ii} are introduced[11].

$$\mathbf{C}_{ij} = \frac{G}{r_{ij}^3} \left[\mathbf{E} - \frac{3(\mathbf{r}_i - \mathbf{r}_j) \otimes (\mathbf{r}_i - \mathbf{r}_j)^T}{r_{ij}^2} \right] \quad i, j = 1, 2, \dots, n, j \neq i \quad (3.26)$$

$$\mathbf{C}_{i0} = \frac{G}{r_i^3} \left[\mathbf{E} - \frac{3(\mathbf{r}_i \otimes \mathbf{r}_i^T)}{r_i^2} \right] \quad i = 1, 2, \dots, n \quad (3.27)$$

$$\mathbf{A}_{ij} = -m_j(-\mathbf{C}_{ij} - \mathbf{C}_{j0}) \quad i, j = 1, 2, \dots, n, j \neq i \quad (3.28)$$

$$\mathbf{A}_{ii} = -(m_0 + m_i)\mathbf{C}_{i0} - \sum_{j=1, j \neq i}^n m_j \mathbf{C}_{ij} \quad i = 1, 2, \dots, n \quad (3.29)$$

The auxiliary matrices \mathbf{A}_{ij} , $i, j = 1, 2, \dots, n$ (of dimension 3×3) can now arranged in one matrix (of dimension $3n \times 3n$)

$$\mathbf{A}_0 = \begin{pmatrix} \mathbf{A}_{11} & \mathbf{A}_{12} & \dots & \mathbf{A}_{1n} \\ \vdots & \vdots & \ddots & \vdots \\ \mathbf{A}_{n1} & \mathbf{A}_{n2} & \dots & \mathbf{A}_{nn} \end{pmatrix} \quad (3.30)$$

Utilizing those matrices, the variational equations assume the standard form

$$\ddot{\mathbf{w}} = \mathbf{A}_0 \mathbf{w} \quad p \in \{p_1, p_2, \dots, p_{6n}\} \quad (3.31)$$

The initial values $\mathbf{w}(t_0), \dot{\mathbf{w}}(t_0)$ are obtained by taking the partial derivatives of the equations defining the initial conditions in the initial value problem. If the parameters refer to any of the masses, either one of the planet's or the solar, the corresponding system of variational equations is inhomogeneous

$$\ddot{\mathbf{w}} = \mathbf{A}_0 \mathbf{w} + \mathbf{f}_p \quad p \in \{m_0, m_1, \dots, m_n\} \quad (3.32)$$

3.5. SHOWCASING IN EXAMPLE SYSTEM

We consider again the Hénon–Heiles system

$$H = \frac{1}{2}(p_x^2 + p_y^2) + \frac{1}{2}(x^2 + y^2) + \left(x^2 y - \frac{1}{3} y^3\right)$$

and its equations of motion that have been computed

$$\begin{aligned} \dot{x} &= p_x & \dot{p}_x &= -x - 2xy \\ \dot{y} &= p_y & \dot{p}_y &= -y - (x^2 - y^2) \end{aligned}$$

Assume a deviation vector $\mathbf{w} = (\delta x, \delta y, \delta p_x, \delta p_y)$. The variational equations governing its evolution can be found by linearizing (differentiating) the equations of motion. Specifically

```
(%i1) qdot1: [p[x], p[y]]
```

```
(%o1) [p_x, p_y]
```

```
(%i2) pdot1: [-2*x*y-x, y^2-y-x^2]
```

```
(%o2) [-2*x*y-x, y^2-y-x^2]
```

```
(%i3) diff(qdot1)
```

```
(%o3) [d(p_x), d(p_y)]
```

```
(%i4) diff(pdot1)
```

```
(%o4) [(-2*y-1)*dx-2*x*dy, (2*y-1)*dy-2*x*dx]
```

which to better show their symmetry can be rewritten

$$\begin{aligned} (\delta \dot{x}) &= \delta p_x & (\delta \dot{p}_x) &= -(1+2y)\delta x - 2x\delta y \\ (\delta \dot{y}) &= \delta p_y & (\delta \dot{p}_y) &= -2x\delta x - (1-2y)\delta y \end{aligned}$$

We again choose the initial conditions:

Type	h	x_0	y_0	\dot{y}_0
regular	0.125	0	0.1	0
chaotic	0.125	0	-0.25	0

Table 3.1.

and we'll be plotting the value $\log \|\mathbf{w}\|$, $\|\mathbf{w}\| = \sqrt{\mathbf{w} \cdot \mathbf{w}}$, $\mathbf{w} = (\delta x, \delta y, \delta p_x, \delta p_y)$. As we'll discuss later this represents a widely used chaos indicator (specifically FLI) in dynamical systems.

```
(%i5) norm(x) := sqrt(x . x)$
```

```
(%i6) normdv(p) :=
      norm(makelist(p[i],i,ceiling(length(p)/2)+1,length(p)))$
```

```
(%i7) x0r: [0,0.1,0.490577890519606,0]$
```

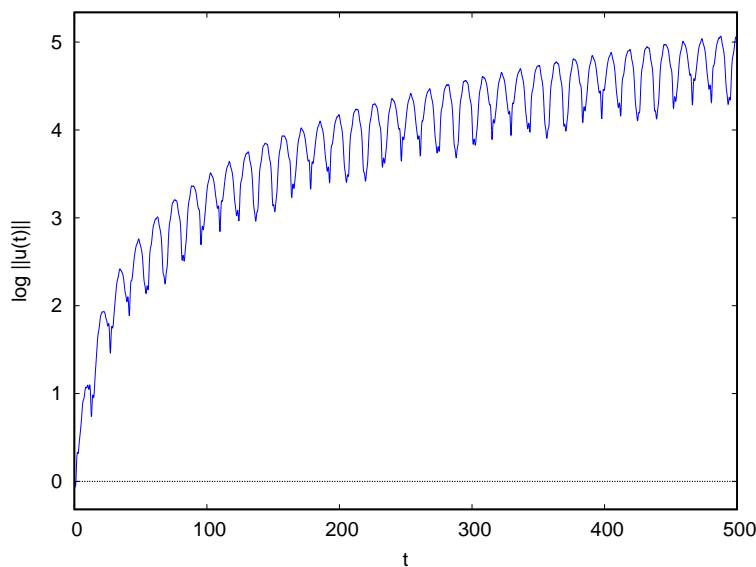
```
(%i8) v0r: x0r/norm(x0r)
```

```
(%o8) [0,0.1997338654842404,0.9798501839458537,0]
```

```
(%i9) X0r: flatten([x0r, v0r])$
```

```
(%i10) solr: rk(
      [px,py,-2*x*y-x,y^2-y-x^2,
       dpx,dpy,(-2*y-1)*dx-2*x*dy,(2*y-1)*dy-2*x*dx],
      [x,y,px,py,dx,dy,dpx,dpy], X0r,
      [t, 0, 500, 0.05])$
```

```
(%i11) tm_plot2d([discrete, makelist(
      [p[1], log(normdv(p))], p, solr)],
      [xlabel, "t"], [ylabel, "log ||u(t)||"])$
```



```
(%i12) x0ir: [0,-0.25,0.4208127057650867,0]$
```

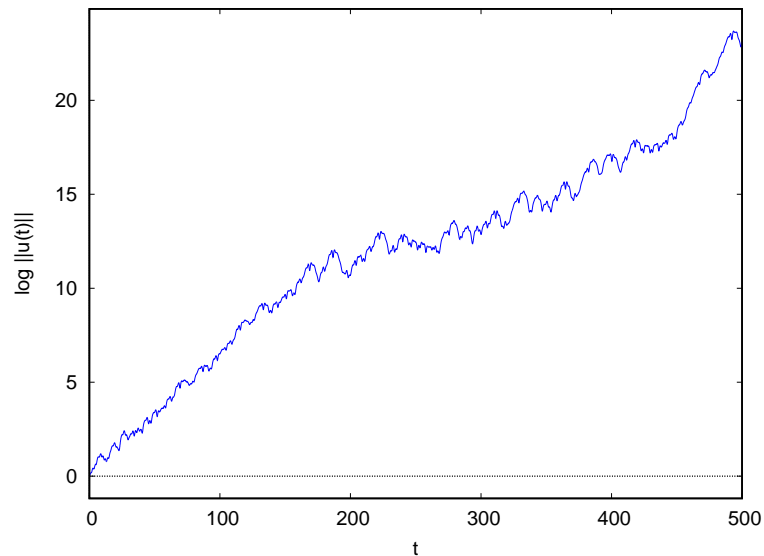
```
(%i13) v0ir: x0ir/norm(x0ir)
```

```
(%o13) [0,-0.5107539184552491,0.8597269536210953,0]
```

```
(%i14) X0ir: flatten([x0ir, v0ir])$
```

```
(%i15) solir: rk(
      [px,py,-2*x*y-x,y^2-y-x^2,
       dpx,dpy,(-2*y-1)*dx-2*x*dy,(2*y-1)*dy-2*x*dx],
      [x,y,px,py,dx,dy,dpx,dpy], X0ir,
      [t, 0, 500, 0.05])$
```

```
(%i16) tm_plot2d([discrete, makelist(  
    [p[1], log(normdv(p))], p, solir)],  
    [xlabel, "t"], [ylabel, "log ||u(t)||"])$
```



We see the difference in behavior for a regular and a chaotic orbit. Whereas for the regular orbit the quantity increases logarithmically (that is there's an increase but remains in low values), for the chaotic it increases linearly in time. The indicator quantifies the qualitative results shown by the images of the trajectories giving thus a tool for stating whether an orbit is regular or chaotic.

CHAPTER 4

STABILITY ANALYSIS

The stability of an orbit of a dynamical system concerns whether nearby orbits will remain in a neighborhood or diverge. Asymptotic stability additionally characterizes attraction of nearby orbits (convergence) in the long-time limit. Stability analysis arises to study and discern the state in the long-time limit of orbits when subjected to small deviations from a reference state[1][14].

Formally, stability means the orbits are located in a bounded region of phase space. If the region is not bounded the orbits could leave the domain through chaotic diffusion. In this case the orbits become unstable. Thus to perform stability investigation of dynamical systems we can detect ordered and chaotic behaviors of the orbits of the system.

That said chaos does not necessarily imply instability[15]. Therefore although we can say that regular orbits lead to stable system doesn't mean chaotic orbits lead to unstable one. An example is the well-studied GJ 876 demonstrating chaotic yet stable motion[16].

Worth noting the related concept of structural stability that concerns stability of the system in perturbations of the map. Briefly a map is structurally stable if “nearby” maps are topologically conjugate to it. In our case the map remains constant and it's the parameters changing.

4.1. CHAOS INDICATORS

As has already been described in introductory chapter, a characteristic of chaotic behavior is the sensitive dependence on initial conditions. For distinguishing between regular and chaotic orbits, numerical tools based on this characteristic have been developed. All subsequently presented indicators are based on the time evolution of deviation (infinitesimal small tangent to the orbit) vectors provided^{4.1} by the variational equations. For this reason those indicators are also referred to as variational indicators.

4.1.1. LCE/LCN

Assuming two trajectories with nearby initial states of distance $\delta_0 = \delta(0)$, their divergence in time will be $\delta(t) \approx e^{\lambda t}$. The exponent λ is called the *Lyapunov characteristic exponent* (LCE), or *maximal Lyapunov exponent* (MLE), and is an indicator showing the mean rate of exponential divergence of nearby trajectories. It's computed[1][18]

$$\lambda = \lim_{t \rightarrow \infty} \frac{1}{t} \log \frac{\delta(t)}{\delta_0} = \lim_{t \rightarrow \infty} \frac{1}{t} \log \frac{\|\mathbf{v}(t)\|}{\|\mathbf{v}_0\|} \quad (4.1)$$

4.1. Alternatively can be calculated by independently evolving a shadow orbit with initial conditions slightly perturbed. But the variational approach has the advantages of being scale-free and circumventing numerical pitfalls associated with the shadow method[17][13].

In general there exists an m -dimensional basis $\{\hat{\mathbf{e}}_i\}$ such that for any \mathbf{v} , λ takes of the m values $\lambda_i = \lambda(\mathbf{x}_0, \mathbf{v}_0; \hat{\mathbf{e}}_i)$. Those values are called simply Lyapunov exponents. In autonomous Hamiltonian system the m exponents are ordered in pairs of opposite sign numbers and two of them are 0. Therefore the computation of λ_1 is sufficient for determining the nature of an orbit[12].

The *Lyapunov characteristic number* (LCN), or *Lyapunov indicator* (LI) or *local Lyapunov exponent* (LLE), is computed after every computational step and is defined as the running average[1][18]

$$\text{LCN}(t_k) = \frac{1}{t_k} \sum_{i=1}^k \log \frac{\|\mathbf{v}_i\|}{\|\mathbf{v}_{i-1}\|} \quad t_k = k \, dt \quad (4.2)$$

To avoid numerical overflow in the lengths of the vectors in case of a chaotic orbits, a re-normalization procedure has to be applied at given intervals (usually after every step) on the tangential vectors. For the initial deviation vector it's common to use the Euclidean norm setting $\delta_0 = \|\mathbf{v}_0\| = 1$.

Theoretically the LCN tends toward the maximal Lyapunov exponent. That is

$$\lim_{k \rightarrow \infty} \text{LCN}(t_k) = \lambda \quad (4.3)$$

The maximal Lyapunov exponent defines the direction to which linearly independent deviation vectors will align for chaotic orbits. Essentially the value λ counts the average exponential divergence around a reference orbit. For a regular orbit $\text{LCN}(t_k) \rightarrow 0$ (no average divergence) whereas for a chaotic orbit $\text{LCN}(t_k) \rightarrow \lambda > 0$ (exponential divergence). Its final value matters and acts as an indicator of the chaos strength[1].

The Lyapunov characteristic number (LCN) is considered reliable indicator for distinguishing regular and chaotic orbits but demands long-time numerical computation especially in case of weak chaos. If only a distinction between regular and chaotic orbits is needed, modifications of it have been developed that give a faster result.

4.1.2. FLI/DFLI

By not re-initializing the deviation vector and retaining only the initial part of the computation of largest LI, we take *fast Lyapunov indicator* (FLI). Originally[19][20] it was conceived as the supremum of the norms of an evolving basis of deviation vectors of initial unitary length but shortly afterwards was replaced by[21][20][1]

$$\text{FLI} = \log \|\mathbf{v}(t)\| \quad (4.4)$$

It's a computationally cheaper definition requiring only one deviation vector of length $\delta(t) = \|\mathbf{v}(t)\|$. It can also distinguish between circulation and libration, something the ordinary LCE cannot do[21][20]. It's defined in such way that FLI/t tends to the largest Lyapunov exponent for $t \rightarrow \infty$, i.e.,

$$\lim_{k \rightarrow \infty} \frac{\text{FLI}}{t} = \lambda$$

For a regular orbit $\frac{d}{dt} \text{FLI} \sim 0$ (slow increase) whereas for a chaotic orbit the increase is significant. Therefore a small value implies a normal evolution whereas a large one implies chaos. Based on previous, the value of FLI to t often appears in literature as the threshold between regularity and chaos[22][23][24].

An improved version to reduce fluctuations is to only retain the largest FLI at each computational step up to this point[25]. Specifically

$$\text{FLI} = \sup_{0 \leq t' \leq t} \log \|\mathbf{v}(t)\| \quad (4.5)$$

Another improvement is to avoid the linear trend of FLI. The *de-trended FLI* (DFLI)[26] can simply be defined as

$$\text{DFLI} = \text{FLI} - \log t = \log \frac{\|\mathbf{v}(t)\|}{t} \quad (4.6)$$

In our later study we'll be computing the DFLI but won't be taking the supremum.

Also worth noting that the FLI and rate of its growth depends on the orientation of the initial vector $\mathbf{v}(t)$. Some studies compute the average (or alternatively the maximum) of the FLIs obtained for an orthonormal basis of tangent vectors[20].

4.1.3. OFLI/2

The *orthogonal fast Lyapunov indicator* (OFLI)[27][28] is variation of FLI that uses the component of deviation vector that is orthogonal to the flow. It was introduced as analogous to the FLI definition reducing fluctuations

$$\text{OFLI} = \sup_{0 \leq t' \leq t} \log \|\mathbf{v}^\perp(t)\| \quad (4.7)$$

An advantage of OFLI is that can distinguish periodicity as it tends to constant value for a periodic orbit, whereas for quasiperiodic and chaotic orbits retains the same behavior as FLI.

An improved version, named OFLI2 method[29][28], to minimize spurious artifacts makes use of 2nd-order variational equations. It's given

$$\text{OFLI2} = \sup_{0 \leq t' \leq t} \log \left\| \left\{ \mathbf{v}(t) + \frac{1}{2} \delta^2 \mathbf{x}(t) \right\}^\perp \right\| \quad (4.8)$$

where with $\delta^{(i)} \mathbf{x}(t)$ we denote the i -th order deviation vectors and having replaced $\delta \mathbf{x}(t) = \mathbf{v}(t)$. Methods based on higher than 1st order variations such as OFLI2 can alleviate problems in systems and initial conditions that Lyapunov exponents may vanish.

Advantages of OFLI can be transferred to other indicators by avoiding the tangent direction in the initial conditions for the variational equations. For Hamiltonian systems such a set of initial conditions can be[30][28]

$$\mathbf{v}_0 = \delta \mathbf{x}_0 = \frac{\nabla H}{\|\nabla H\|} \quad (4.9)$$

And in Hamiltonian systems with 1 d.o.f this is the only choice available. In cases of more d.o.f other choices are utilizing random initial conditions, and basically in cases of systems with many d.o.f. such as the n -body problem can simply take $v_0^{(1)} = 1, v_0^{(i)} = 0, i > 1$ that is $\mathbf{v}_0 = (1, 0, 0, \dots, 0)$, or evolve multiple deviation vectors as already mentioned is done regarding FLI.

4.1.4. MEGNO

The *mean exponential growth of nearby orbits* (MEGNO) initially introduced while studying dynamics in non-axisymmetric galactic potentials[31], was later formalized as a technique on its own[32]. As will be detailed is both a fast indicator and can provide an estimate of the LCN converging to the null value faster than the classical algorithm[31][33].

We first rewrite LCN in integral form.

$$\text{LCN}(t) = \frac{1}{t} \int_0^t \frac{\|\mathbf{v}(t')\|}{\|\mathbf{v}_0\|} dt' = \left\langle \frac{\|\mathbf{v}(t)\|}{\|\mathbf{v}_0\|} \right\rangle \quad (4.10)$$

Then MEGNO is defined as the quantity

$$Y(t) = \frac{2}{t} \int_0^t t' \frac{\delta(t')}{\delta(t')} dt' = \frac{2}{t} \int_0^t t' \frac{\|\dot{\mathbf{v}}(t')\|}{\|\mathbf{v}(t')\|} dt' \quad (4.11)$$

and for discrete time systems

$$Y(n) = \frac{2}{n} \sum_{j=1}^n j \log \frac{\|\mathbf{v}_j\|}{\|\mathbf{v}_{j-1}\|} \quad (4.12)$$

Essentially MEGNO introduces a time weight giving larger weight to values taken at longer times. Then the continuous quantity for computational purposes can be rewritten as the running sum

$$Y(t_k) = \frac{2}{t_k} \sum_{i=1}^k t_i \log \frac{\|\mathbf{v}_i\|}{\|\mathbf{v}_{i-1}\|} \quad t_j = j dt \quad (4.13)$$

It's proved[33] that for a regular orbit is approximated

$$Y_r(t) \approx 2 - \frac{2 \ln(1 + \lambda_r t)}{\lambda_r t} + \mathcal{O}(\chi_r(t)) \quad (4.14)$$

Introducing the time average

$$\bar{Y}_r(t) = \frac{1}{t} \int_0^t Y_r(t') dt' \Rightarrow \bar{Y}_r = \lim_{t \rightarrow \infty} \bar{Y}_r(t) = 2 \quad (4.15)$$

For a chaotic orbit is approximated

$$Y_{\text{ir}}(t) \approx \lambda_{\text{ir}} t + \mathcal{O}(\chi_{\text{ir}}(t)) \quad (4.16)$$

and averaging

$$\bar{Y}_{\text{ir}} = \lim_{t \rightarrow \infty} \bar{Y}_{\text{ir}}(t) = \lim_{t \rightarrow \infty} \frac{\lambda_{\text{ir}} t}{2} \rightarrow \infty \quad (4.17)$$

Hence for regular orbits MEGNO is osculating around 2 for finite time spans but tends to a constant value for time tending to infinity, whereas for chaotic orbits it's increasing linearly in time. Note that since $\frac{d}{dt} \bar{Y}_{\text{ir}} \sim \lambda_{\text{ir}}/2$ it's possible to get, by linear fitting $\bar{Y}_{\text{ir}}(t)$, an accurate estimate for LCE in shorter times than classical algorithm which approaches by $\log t/t$.

Overall, the time average can take the general form

$$\bar{Y}(t) = at + b \quad (4.18)$$

with values depending on the motion given in the following table.

irregular / chaotic motion	$a = \lambda/2, b \approx 0$
quasiperiodic motion	$a = 0, b \approx 2$
stable periodic orbits	$b \lesssim 2$
unstable periodic orbits	$b \gtrsim 2$

MEGNO exhibits an analytical relation with FLI[34][33]. The time averaged FLI is given

$$\overline{\text{FLI}}(t) = \frac{1}{t} \int_0^t \log \delta(t') dt' \quad (4.19)$$

From the definition of MEGNO, assuming $\delta_0 = 1$

$$Y(t) = \frac{2}{t} \int_0^t t' \frac{d}{dt'} [\log \delta(t')] dt' = 2 \left[\ln \delta(t) - \frac{1}{t} \int_0^t \log \delta(t') dt' \right] \quad (4.20)$$

And comparing with previous

$$Y(t) = 2[\text{FLI}(t) - \overline{\text{FLI}}(t)] \quad (4.21)$$

Hence MEGNO is twice the difference between FLI and its time average over the interval $(0, t)$. This highlight two points regarding MEGNO. It (i) takes advantage of the dynamical information of the evolution of the tangent vector along the complete orbit, and (ii) shows why it distinguishes chaos at absolute scale (regular orbits tend asymptotically to^{4.2} 2) whereas FLI at relative.

For discrete-time systems the relation is slightly different. Since we're essentially using the discrete algorithm, it's worth mentioning this as well. The average FLI in this case is

$$\overline{\text{FLI}}(n) = \frac{1}{n} \sum_{j=0}^n \log \|\mathbf{v}_j\| = \frac{1}{n} \sum_{j=0}^n \log \delta(j) \quad (4.22)$$

and from the definition of MEGNO[34]

$$\begin{aligned} Y(n) &= \frac{2}{n} \left[\sum_{j=1}^n j \log \delta(j) - \sum_{j=1}^n j \log \delta(j-1) \right] \\ &= \frac{2}{t} \left[\sum_{j=1}^n j \log \delta(j) - \sum_{j=1}^{n-1} j \log \delta(j-1) \right] \\ &= 2 \left[\log \delta(n) - \frac{1}{n} \sum_{j=0}^n \log \delta(j) + \frac{1}{t} \log \delta(n) \right] \\ &= 2[\text{FLI}(n) - \overline{\text{FLI}}(n)] + (2/t) \log \delta(n) \end{aligned} \quad (4.23)$$

So we find the relation is similar but with an error of order λ , that is,

$$Y(n) = 2[\text{FLI}(n) - \overline{\text{FLI}}(n)] + \mathcal{O}(\lambda) \quad (4.24)$$

4.1.5. SALI/GALI

Let's assume two deviation vectors $\mathbf{v}_1, \mathbf{v}_2$ for an orbit. For chaotic orbits the two initially different deviation vectors tend to coincide with the direction defined by the maximal Lyapunov exponent.

^{4.2} The actual value is of course determined by the arbitrarily chosen multiplication factor of the integral in the definition. Nevertheless the dynamic picture is the same regardless of which factor is chosen.

Upon this the *smaller alignment index* (SALI)[35][36] can be introduced. It's defined, with $\mathbf{v}_1, \mathbf{v}_2$ defining an orthonormal basis of deviation vectors,

$$\text{SALI} = \min \{ \|\hat{\mathbf{v}}_1 - \hat{\mathbf{v}}_2\|, \|\hat{\mathbf{v}}_1 + \hat{\mathbf{v}}_2\| \} \quad \hat{\mathbf{v}}_i = \frac{\mathbf{v}_i}{\|\mathbf{v}_i\|} \quad (4.25)$$

which means

$$\|\hat{\mathbf{v}}_1 - \hat{\mathbf{v}}_2\| \leq \text{SALI} \leq \|\hat{\mathbf{v}}_1 + \hat{\mathbf{v}}_2\| \Rightarrow 0 \leq \text{SALI} \leq \sqrt{2} \quad (4.26)$$

For chaotic orbits

$$\text{SALI}(t) \propto e^{-(\lambda_1 - \lambda_2)t} \rightarrow 0$$

whereas for regular orbits it fluctuates around a value within the interval $(0, \sqrt{2}]$.

Geometrically, SALI effectively measures the area of the parallelogram formed by the two deviation vectors. Specifically

$$A = \|\hat{\mathbf{v}}_1 \wedge \hat{\mathbf{v}}_2\| = \frac{\|\hat{\mathbf{v}}_1 - \hat{\mathbf{v}}_2\| \|\hat{\mathbf{v}}_1 + \hat{\mathbf{v}}_2\|}{2} = \text{SALI} \cdot \frac{\max \{ \|\hat{\mathbf{v}}_1 - \hat{\mathbf{v}}_2\|, \|\hat{\mathbf{v}}_1 + \hat{\mathbf{v}}_2\| \}}{2} \Rightarrow A \propto \text{SALI} \quad (4.27)$$

Therefore an alternative definition simply sets it equal to the area[36]. That is^{4.3}

$$\text{SALI} = \sqrt{2}A = \sqrt{2}\|\hat{\mathbf{v}}_1 \wedge \hat{\mathbf{v}}_2\| = \sqrt{2} \sin(\phi) \quad (4.28)$$

where we set the multiplication factor $\sqrt{2}$ (also similar to MEGNO which also has an arbitrarily chosen multiplication factor) so the result coincides with original definition. The essential part though is that for chaotic motion it exponentially tends to zero whereas for regular orbits it fluctuates around non-zero values.

Based on this the *generalized alignment index* (GALI)[37][36] is introduced and for $2n$ -dimensional space extends SALI to k deviation vectors such that $2 \leq k \leq 2n$.

$$\text{GALI}_k = \|\hat{\mathbf{v}}_1 \wedge \dots \wedge \hat{\mathbf{v}}_k\| \quad (4.29)$$

For chaotic orbits

$$\text{GALI}_k \propto e^{-\{\sum(\lambda_1 - \lambda_j)\}t} \rightarrow 0$$

The relation is valid even if some Lyapunov exponents are equal or close to each other. As can be seen SALI is just the form GALI takes for $k=2$ or more precisely, and considering the multiplication factor, $\text{SALI} = \sqrt{2} \text{GALI}_2$.

4.1.6. RLI

Let's assume two nearby orbits. If those are regular then the LCN is expected to have a similar evolution for both such that over time the difference tends towards zero. If those are chaotic then difference will be non-zero.

Upon this the *relative Lyapunov indicator* (RLI)[38][24] can be introduced. Instead of computing LCN for a large time scale, it's computed for two nearby orbits (the "base" and its "shadow") separated by distance δx . Then RLI is defined as

$$\text{RLI}(t; x_0) = |\text{LCN}(t; x_0 + \delta x) - \text{LCN}(t; x_0)| \quad (4.30)$$

^{4.3.} Although $\hat{\mathbf{v}}_1 \wedge \hat{\mathbf{v}}_2$ and $\hat{\mathbf{v}}_1 \times \hat{\mathbf{v}}_2$ mathematically correspond to different entities, it's $\|\hat{\mathbf{v}}_1 \wedge \hat{\mathbf{v}}_2\| = \|\hat{\mathbf{v}}_1 \times \hat{\mathbf{v}}_2\|$. Therefore the definition could alternatively use the cross rather wedge product. For more regarding exterior algebra and the wedge product can refer to [18].

To eliminate the high frequency fluctuation, the smoothed (averaged) $\overline{\text{RLI}}$ defined as

$$\overline{\text{RLI}}(t_k) = \langle \text{RLI}(t_k; x_0) \rangle_t = \frac{1}{t_k} \sum_{i=1}^k \text{RLI}(t_i; x_0) \quad t_j = i \, dt \quad (4.31)$$

is more preferred[24]. The values for chaotic motion are several orders of magnitude higher than for regular motion. The distance δx is chosen arbitrarily depending on the problem studied and should be small enough to reflect the local properties of the phase space. Alongside the need for a threshold means RLI has two free parameters. For ordered orbits it shows linear dependence on δx but for chaotic orbits it's practically invariant to the choice made. Thus the choice of δx does not modify essentially the behavior of the RLI[24].

4.2. SHOWCASING IN EXAMPLE SYSTEM

We consider again the Hénon–Heiles system

$$H = \frac{1}{2}(p_x^2 + p_y^2) + \frac{1}{2}(x^2 + y^2) + \left(x^2 y - \frac{1}{3} y^3 \right)$$

Its equations of motion and variational equations for deviation vector $\mathbf{w} = (\delta x, \delta y, \delta p_x, \delta p_y)$ are

$$\begin{aligned} \dot{x} &= p_x & \dot{p}_x &= -x - 2xy \\ \dot{y} &= p_y & \dot{p}_y &= -y - (x^2 - y^2) \\ (\delta \dot{x}) &= \delta p_x & (\delta \dot{p}_x) &= -(1 + 2y)\delta x - 2x\delta y \\ (\delta \dot{y}) &= \delta p_y & (\delta \dot{p}_y) &= -2x\delta x - (1 - 2y)\delta y \end{aligned}$$

Hénon–Heiles system has been extensively studied in literature. Related to orbit classification someone can read [39] and references within. We will only show the evolution of the indicators for a regular and a chaotic orbit but no commentary will be given other than what discussed above.

The comparative study of them will take place in the later section with the numerical integration of a 3-planet system. Such study for HH system can be found in [23][24]. A similar but for few other 4d maps can be found in [22], and for few 2d dynamical systems in [40].

We again choose the initial conditions:

Type	h	x_0	y_0	y_0
regular	0.125	0	0.1	0
chaotic	0.125	0	-0.25	0

Table 4.1.

```
(%i17) zip(lst1, lst2) := makelist([lst1[i], lst2[i]], i, 1, length(lst1))$
```

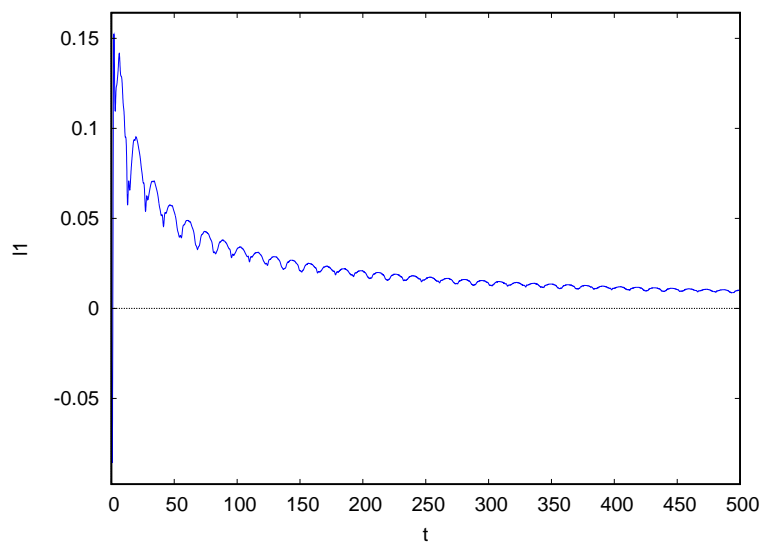
```
(%i18) tlst: makelist(p[1], p, solr)$
```

```
(%i19) ratprint: false$
```

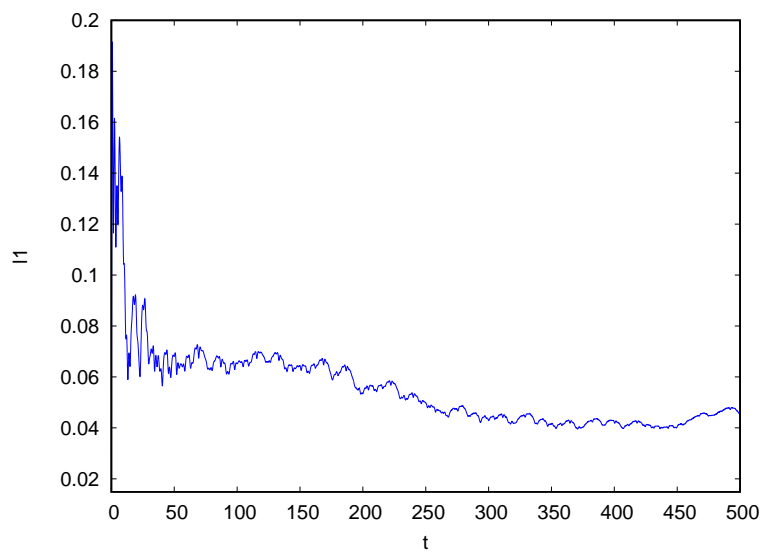
4.2.1. LCE/LCN

We plot the temporal evolution of λ_1 . To get an approximate value for λ in case of chaotic orbit we can perform a linear fit to the near-linear part.

```
(%i20) tm_plot2d([discrete, makelist(
    [p[1], log(normdv(p))/p[1]], p, rest(solr))],
    [xlabel, "t"], [ylabel, "l1"])$
```



```
(%i21) tm_plot2d([discrete, makelist(
    [p[1], log(normdv(p))/p[1]], p, rest(solir))],
    [xlabel, "t"], [ylabel, "l1"])$
```

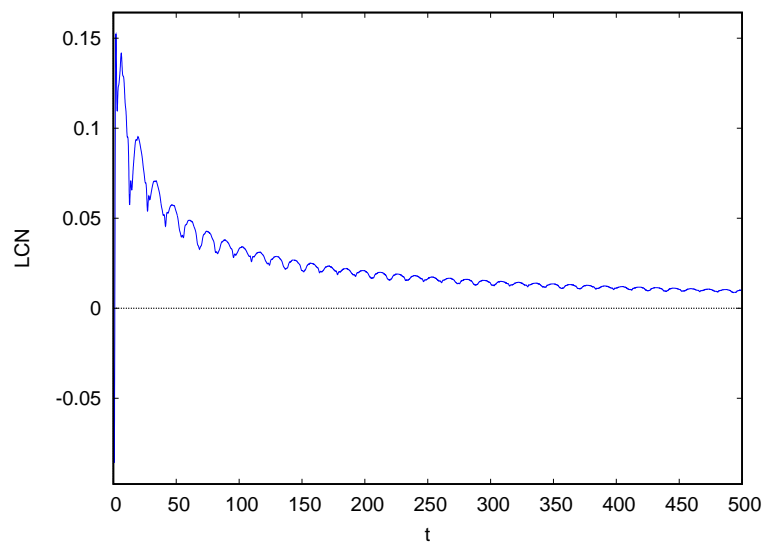


Then we plot the temporal evolution of LCN. Since here we cannot renormalize after each computational step we compute via the following routine that replicates this after the entire computation has run^{4.4}.

```
(%i22) lcn(norms) := block([res : [], s : 0, prev : 1],
  while norms # [] do (
    ksi : first(norms),
    s : log(ksi/prev) + s,
    prev : ksi,
    norms : rest(norms),
    res : cons(s, res)),
  reverse(res))$
```

```
(%i23) normsr: makelist(normdv(p), p, solr)$
```

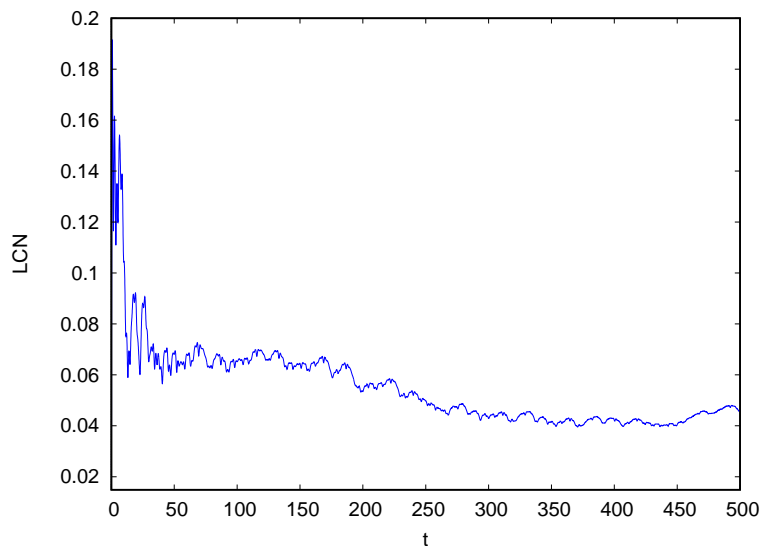
```
(%i24) tm_plot2d([discrete, makelist(
  [p[1], p[2]/p[1]], p, rest(zip(tl1st, lcn(normsr)))]),
  [xlabel, "t"], [ylabel, "LCN"])$
```



```
(%i25) normsir: makelist(normdv(p), p, solir)$
```

4.4. Based on a blog comment by S. Macrakis about implementing an efficient cumulative sum on Maxima.

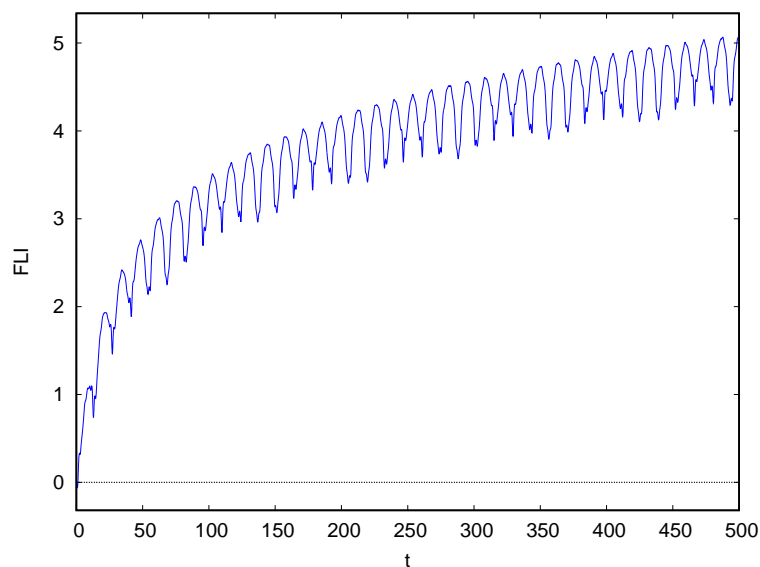
```
(%i26) tm_plot2d([discrete, makelist(
    [p[1], p[2]/p[1]], p, rest(zip(tlst, lcn(normsir))))],
    [xlabel, "t"], [ylabel, "LCN"])$
```



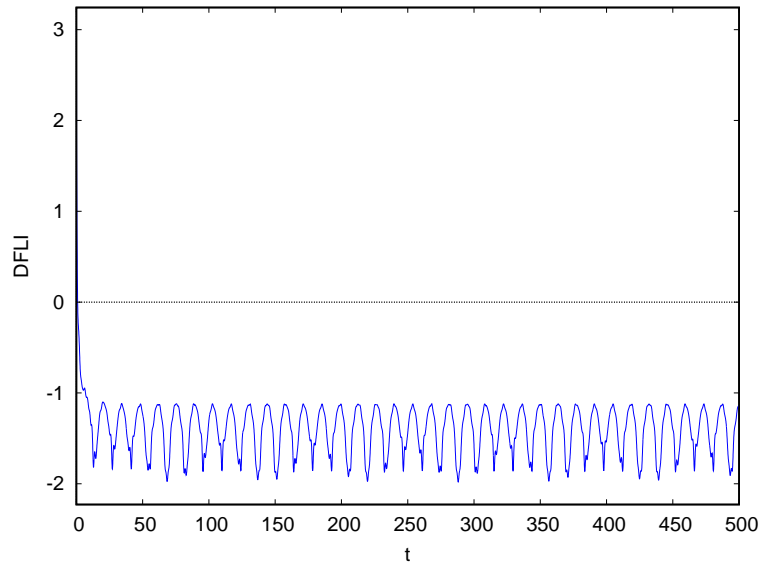
4.2.2. FLI/DFLI

The plots shown as example in the variational equations chapter actually correspond to FLI. We plot them again to compare to DFLI. Notice how DFLI has no linear trend.

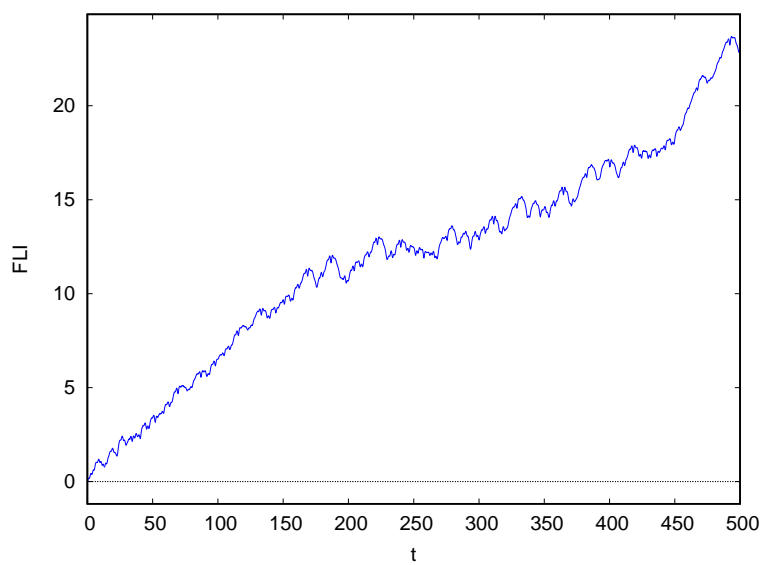
```
(%i27) tm_plot2d([discrete, makelist(
    [p[1], log(normdv(p))], p, rest(solr))],
    [xlabel, "t"], [ylabel, "FLI"])$
```



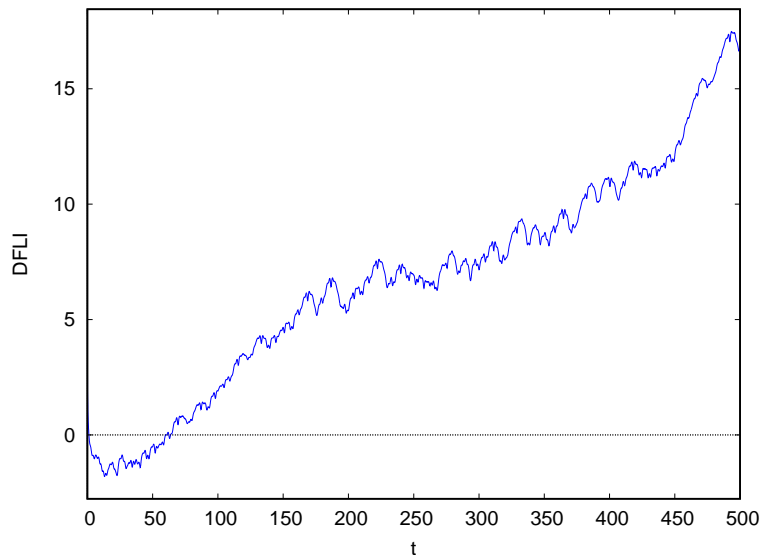
```
(%i28) tm_plot2d([discrete, makelist(  
    [p[1], log(normdv(p)/p[1])], p, rest(solr))],  
    [xlabel, "t"], [ylabel, "DFLI"])$
```



```
(%i29) tm_plot2d([discrete, makelist(  
    [p[1], log(normdv(p))], p, rest(solir))],  
    [xlabel, "t"], [ylabel, "FLI"])$
```



```
(%i30) tm_plot2d([discrete, makelist(
    [p[1], log(normdv(p)/p[1])], p, rest(solir)]),
    [xlabel, "t"], [ylabel, "DFLI"])$
```



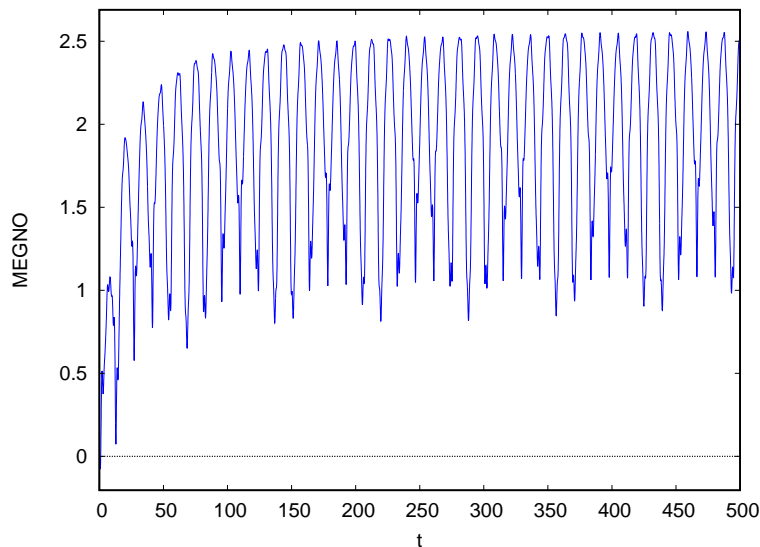
4.2.3. MEGNO

Similar to LCN here we cannot renormalize or apply the time weight after each computational step, so we compute via the following routine that replicates this after the entire computation has run.

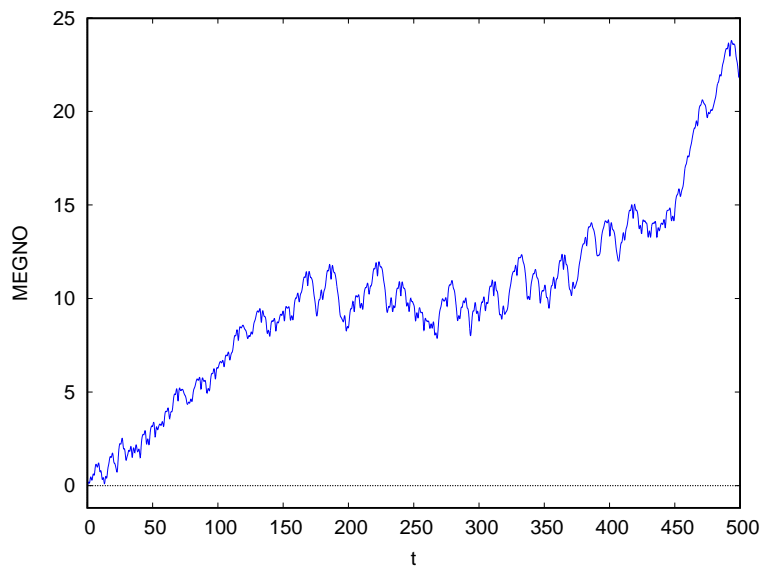
```
(%i31) megno(t, norms) := block([res : [], s : 0, prev : 1],
    while (t, norms) # [] do (
        ksi : first(norms),
        s : first(t)*log(ksi/prev) + s,
        prev : ksi,
        norms : rest(norms),
        t : rest(t),
        res : cons(s, res)),
    reverse(res))$
```



```
(%i32) tm_plot2d([discrete, makelist(
    [p[1], 2*p[2]/p[1]], p, rest(zip(tlst, megn(tlst, normsr))))],
    [xlabel, "t"], [ylabel, "MEGNO"])$
```



```
(%i33) tm_plot2d([discrete, makelist(
    [p[1], 2*p[2]/p[1]], p, rest(zip(tlst, megn(tlst, normsir))))],
    [xlabel, "t"], [ylabel, "MEGNO"])$
```



4.2.4. SALI

To compute SALI we've to evolve two deviation vectors. The simplest will be evolve two orbits with different set of initial conditions for the deviation vector. This will sub-optimal implementation since we will be solving the primary equations twice whereas the difference

lies only in the variational equations. So what we're doing is we introduce an extra set of variational equations with $(\delta q)', (\delta p_q)'$ rather $(\delta q), (\delta p_q)$ that'll evolve the other deviation vector.

```
(%i34) uv(vec) := vec/norm(vec)$
```

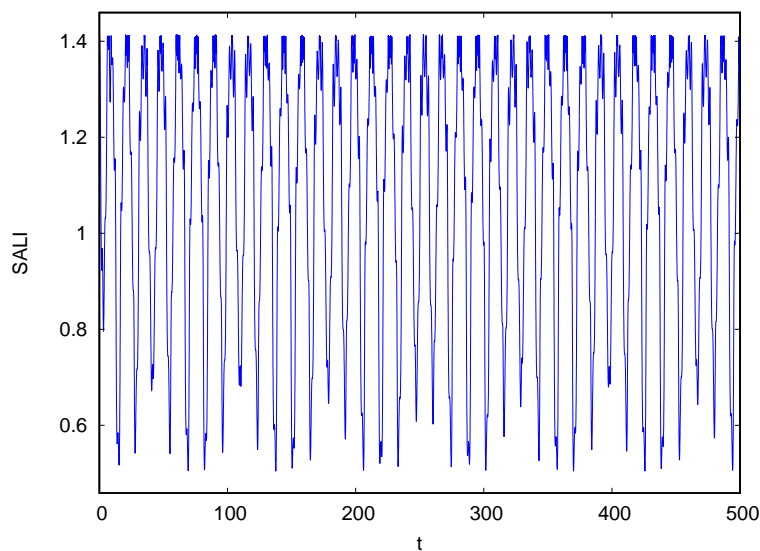
```
(%i35) solsr: rk(
  [px,py,-2*x*y-x,y^2-y-x^2,
   dpx,dpy,(-2*y-1)*dx-2*x*dy,(2*y-1)*dy-2*x*dx,
   dpx1,dpy1,(-2*y-1)*dx1-2*x*dy1,(2*y-1)*dy1-2*x*dx1],
  [x,y,px,py,dx,dy,dpx,dpy,dx1,dy1,dpx1,dpy1],
  [0,0.1,0.490577890519606,0,1,0,0,0,0,1,0,0],
  [t, 0, 500, 0.05])$
```

```
(%i36) u1: makelist(uv([p[6], p[7], p[8], p[9]]), p, solsr)$
```

```
(%i37) u2: makelist(uv([p[10], p[11], p[12], p[13]]), p, solsr)$
```

```
(%i38) sali: makelist(
  min(norm(u1[i]-u2[i]),norm(u1[i]+u2[i])),i,1,length(u1))$
```

```
(%i39) tm_plot2d([discrete, zip(tlst, sali)],
  [xlabel, "t"], [ylabel, "SALI"])$
```



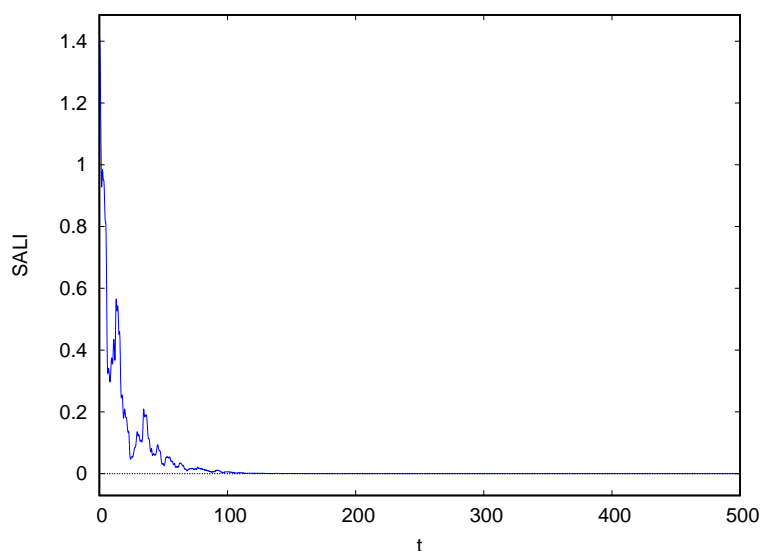
```
(%i65) solsir: rk(
    [px,py,-2*x*y-x,y^2-y-x^2,
     dpx,dpy,(-2*y-1)*dx-2*x*dy,(2*y-1)*dy-2*x*dx,
     dpx1,dpy1,(-2*y-1)*dx1-2*x*dy1,(2*y-1)*dy1-2*x*dx1],
    [x,y,px,py,dx,dy,dpx,dpy,dx1,dy1,dpx1,dpy1],
    [0,-0.25,0.4208127057650867,0,1,0,0,0,0,0,1,0,0],
    [t, 0, 500, 0.05])$

(%i66) u1: makelist(uv([p[6], p[7], p[8], p[9]]), p, solsir)$

(%i67) u2: makelist(uv([p[10], p[11], p[12], p[13]]), p, solsir)$

(%i68) sali: makelist(
    min(norm(u1[i]-u2[i]),norm(u1[i]+u2[i])),i,1,length(u1))$

(%i69) tm_plot2d([discrete, zip(tlst, sali)],
    [xlabel, "t"], [ylabel, "SALI"])$
```



4.2.5. RLI

```
(%i45) X1r: copylist(X0r)$

(%i46) X1r[1]: X0r[1]+10e-10$

(%i47) solr1: rk(
    [px,py,-2*x*y-x,y^2-y-x^2,
     dpx,dpy,(-2*y-1)*dx-2*x*dy,(2*y-1)*dy-2*x*dx],
    [x,y,px,py,dx,dy,dpx,dpy], X1r,
    [t, 0, 500, 0.05])$

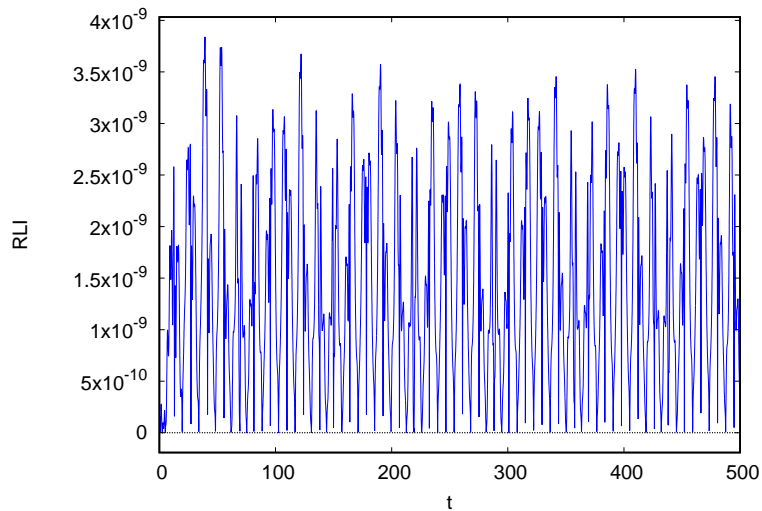
(%i48) lcn0r: lcn(normsr)$

(%i49) normsr1: makelist(normdv(p), p, solr1)$

(%i50) lcn1r: lcn(normsr1)$

(%i51) rli: abs(lcn0r-lcn1r)$
```

```
(%i52) tm_plot2d([discrete, zip(tlst, rli)],
  [xlabel, "t"], [ylabel, "RLI"])$
```



```
(%i53) X1ir: copylist(X0ir)$
```

```
(%i54) X1ir[1]: X1ir[1]+10e-10$
```

```
(%i55) solir1: rk(
  [px,py,-2*x*y-x,y^2-y-x^2,
   dpx,dpy,(-2*y-1)*dx-2*x*dy,(2*y-1)*dy-2*x*dx],
  [x,y,px,py,dx,dy,dpx,dpy], X1ir,
  [t, 0, 500, 0.5])$
```

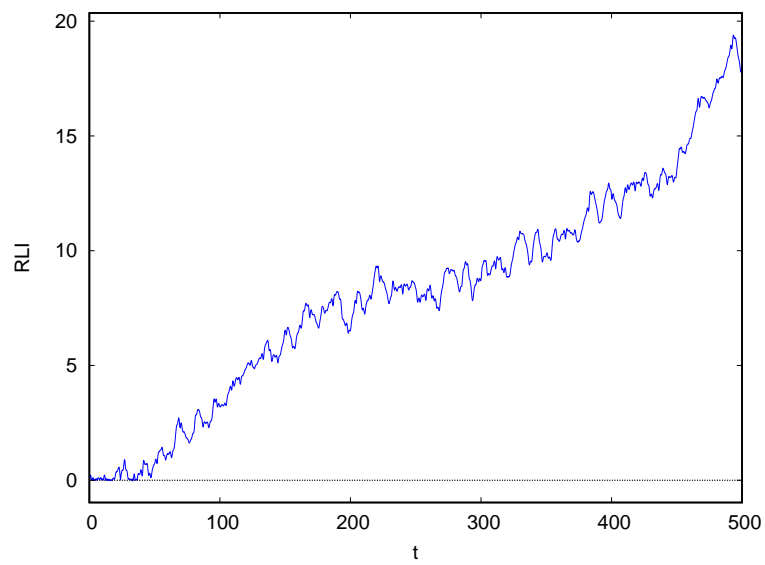
```
(%i56) lcn0ir: lcn(normsir)$
```

```
(%i57) normsir1: makelist(normdv(p), p, solir1)$
```

```
(%i58) lcn1ir: lcn(normsr1)$
```

```
(%i59) rli: abs(lcn0ir-lcn1ir)$
```

```
(%i60) tm_plot2d([discrete, zip(tlst, rli)],  
                [xlabel, "t"], [ylabel, "RLI"])$
```



CHAPTER 5

NUMERICAL INTEGRATIONS

Having introduced the necessary theory and having shown some examples, we proceed to applying that theory to the 3-planet problem (4-body n -problem), that is 3 bodies in orbit around a more massive one. We'll study the chaos in a 3-planet system computing the indicators DFLI, MEGNO, SALI, and RLI. Our objective is to compare those indicators as fast predictors to a planetary system's stability. The OFLI is excluded as we aren't looking to discern periodic orbits specifically and is having the same behavior with FLI otherwise.

For the integration an in-house code originally written for the 2-planet problem is modified for usage in the 3-planet problem. Rather utilizing variable arrays and therefore converting it to an n -planet integrator, the expressions for the 3-planet problem are hardcoded. The reason behind this being that it's a specific problem and static variables result in better performance, something welcomed as long integrations are required for such study.

For the study, we've chosen, based on values commonly used in literature[26][22][23][24], max DFLI to be 30 (31 in case of error), max MEGNO to be 7 (8 in case of error)^{5.1}, min SALI to be 10^{-4} (0 in case of error), and max RLI to be 10^{-4} (0 in case of error) with separation set to 10^{-10} . For all integrations the energy and angular momentum are accurate to 10^{-11} .

The studied system is HD 82943^{5.2}. It was for many years known to harbor two planets and, although had been previously suggested[41][42], only recently good indications for a third one were found[15]. Numerical simulations have shown the inner two-planet system, planets b and c , to reside in stable resonant state[43][44][45], specifically an apsidal corotation resonance^{5.3}. But the dynamical status of planet d is uncertain as of latest observational data. It may reside in as well as slightly out of the 5:2 resonance. The orbital period and minimum masses have been found but the eccentric parameters are uncertain[15].

The system has a host star with mass $1.18 M_{\text{Sun}}$ and planets with masses and orbital elements given in the following table^{5.4}.

Planet	m (M_{Jup})	a (AU)	e	i (deg)	Ω (deg)	ω (deg)	M (deg)
b	4.78	0.746	0.425	19.4	0	133	NA
c	4.8	1.190	0.203	19.4	0	107	NA
d	0.29	2.145	0.001	19.4	0	NA	NA

Table 5.1.

5.1. Since for regular orbits MEGNO oscillates around 2, we've to pick a value higher than it to make sure we don't classify as chaotic a regular orbit.

5.2. As trivia HD 82943 is at distance $d = 22.46$ pc from us and it has a G0 type host star.

5.3. Apsidal corotation resonance refers to simultaneous apsidal alignment and mean-motion resonance[43].

5.4. Data taken from exoplanet.eu. Note that data for 2-planet system b, c and d in database are from different papers. A fancy plot made using REBOUND package of the orbits for those initial conditions setting $w_d = 180$ deg, $M_j = 0 \forall j$ can be seen on the cover of this thesis.

Note that the actual masses found observationally are $m \sin i$. The data above consider this and with i known give m . Nevertheless this is the minimum mass for the body.

Since system is coplanar we set $i_j = 0$ and to make the comparative study of chaotic indicators simpler we set $\Omega_j = \omega_j = 0 \forall j$ and $M_b = M_c = 0$. That is planets b and c are set in alignment at the start of the integration, something that can be done due to them known to be in apsidal alignment with $\Delta\varpi(t') = 0$. Then we start by studying the position of planet d .

We generate $a_d - M_d$ stability maps for $a_d \in [1.5, 3.0]$, $M_d \in [0, 360]$. The maps are shown for times 10^4 years.

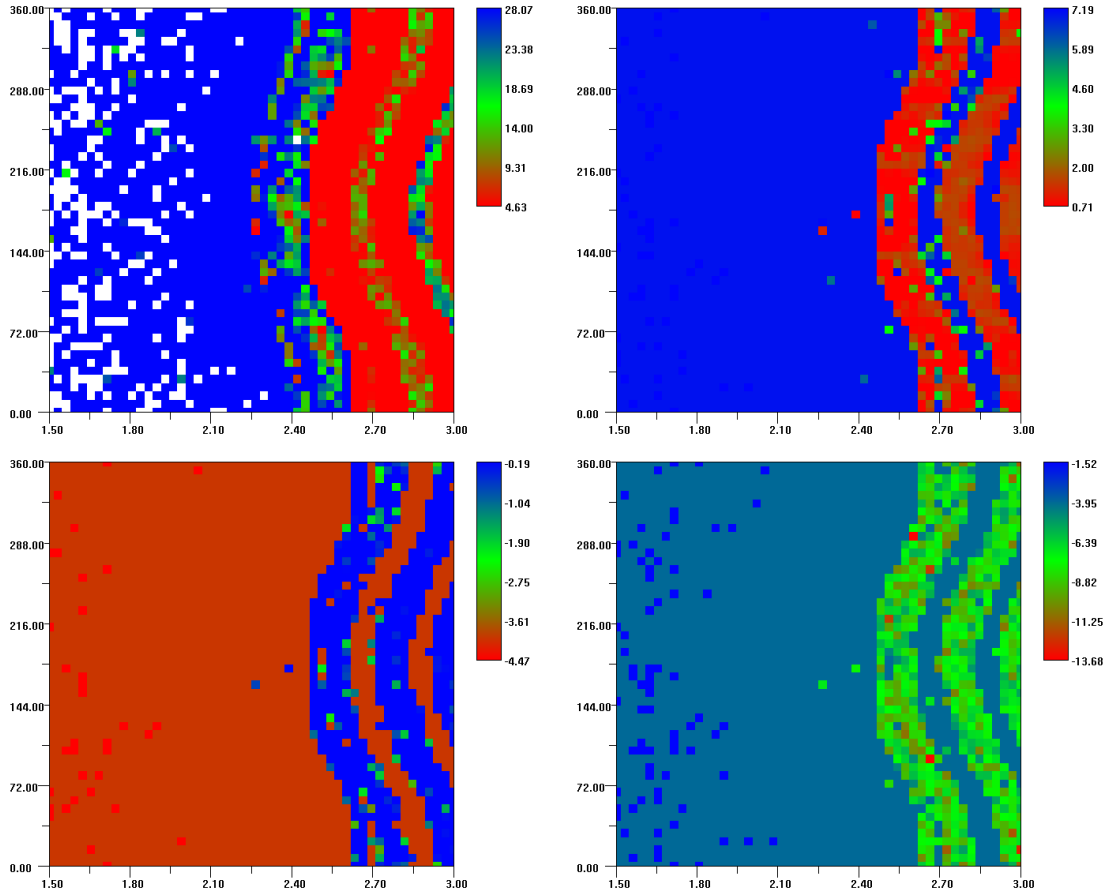


Figure 5.1. (top) DFLI left, MEGNO right, (bottom) log SALI left, log RLI right. The white spots show when integration has failed, i.e., a collision has occurred. The (x, y) axis are (a_d, M_d) respectively.

We choose the following regular and chaotic parameters.

Type	a_d	M_d
regular	2.52	180.0
chaotic	2.42	180.0

Table 5.2. Regular and chaotic orbit for $e_d = 0.001$.

The evolution of a, e ($i = \text{const.}$) for regular orbit is

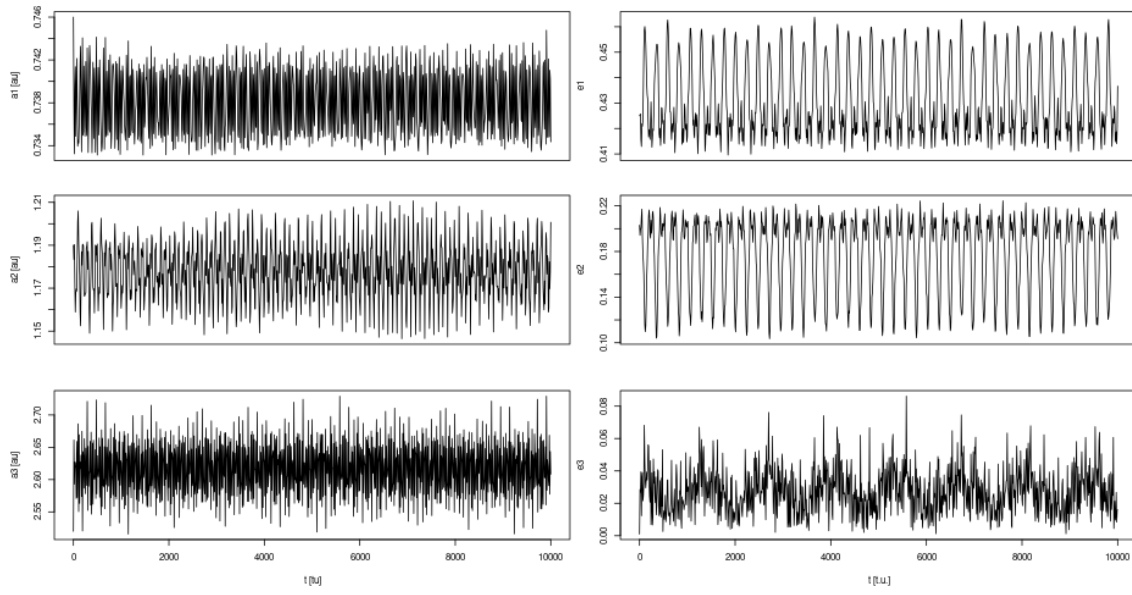


Figure 5.2. Evolution of a, e for regular orbit $(a_d, M_d) = (2.52, 180)$.

The evolution of a, e ($i = \text{const.}$) for chaotic orbit is

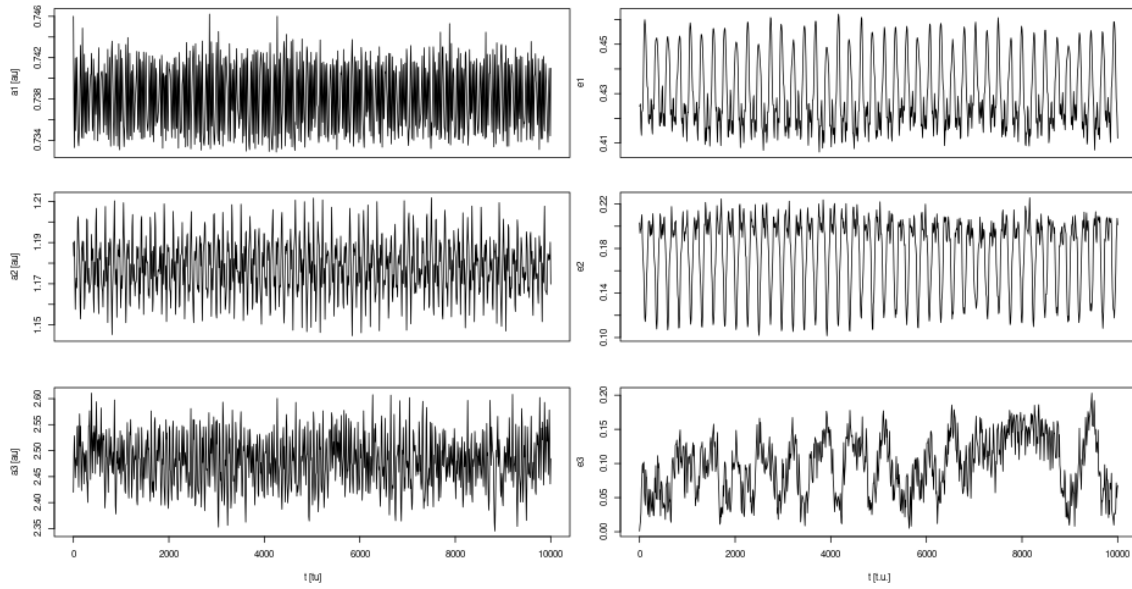


Figure 5.3. Evolution of a, e for chaotic orbit $(a_d, M_d) = (2.42, 180)$.

The evolution of the indicators is then taken to the end without early breaking in the case of chaotic orbit.

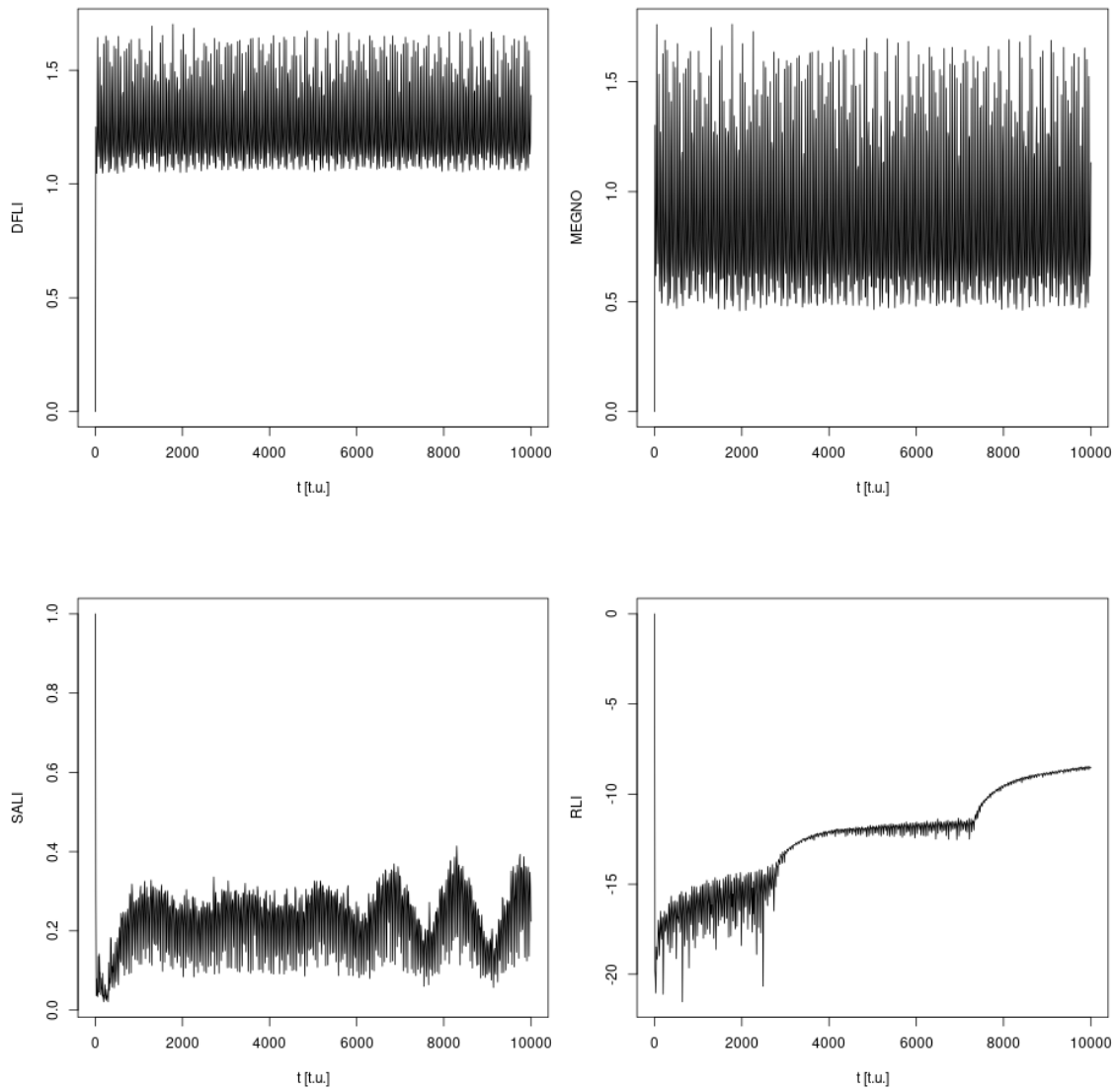


Figure 5.4. Evolution of DFLI, MEGNO, SALI, log RLI for for regular orbit $(a_d, M_d) = (2.52, 180)$.

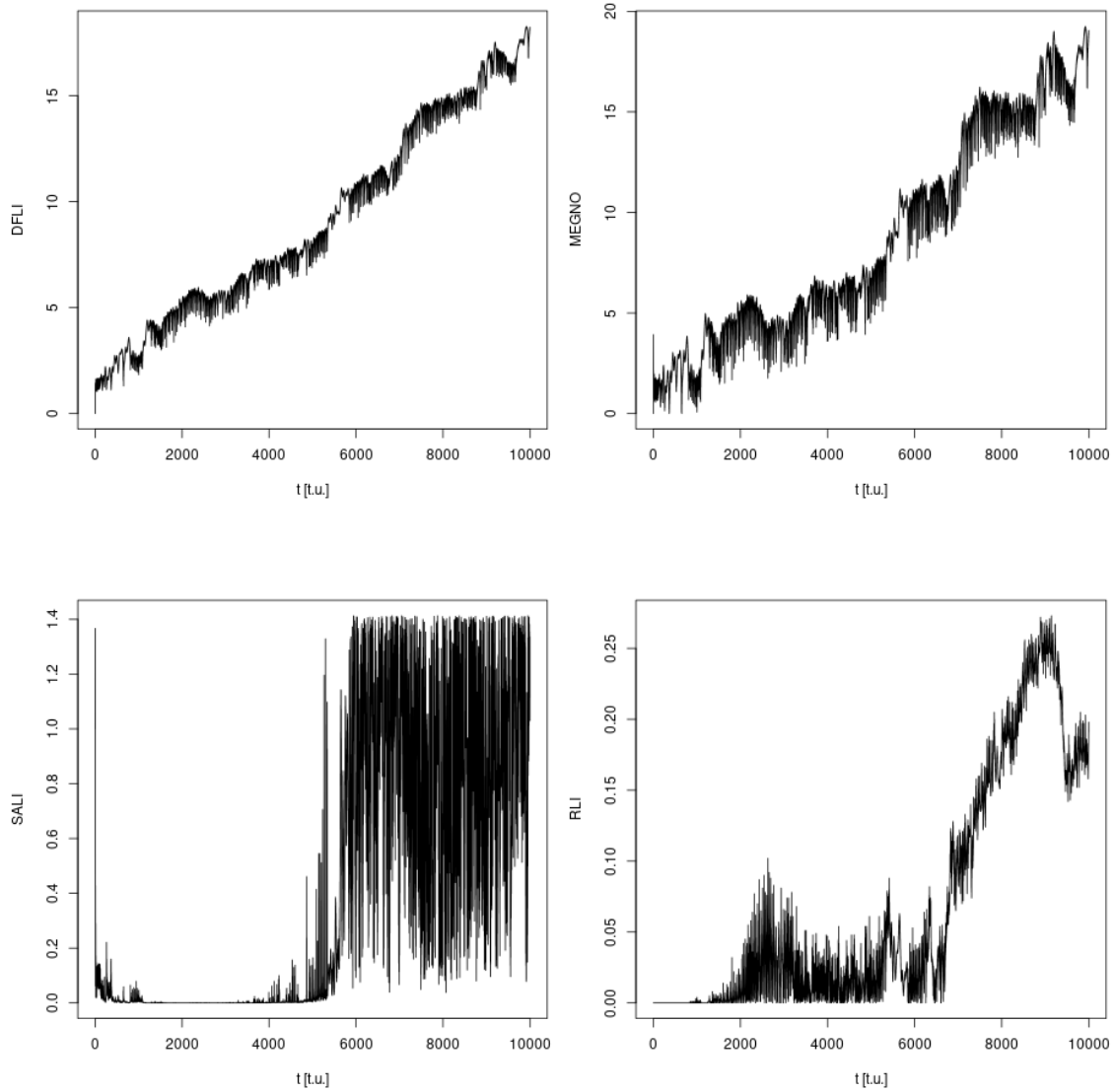


Figure 5.5. Evolution of DFLI, MEGNO, SALI, RLI for for chaotic orbit $(a_d, M_d) = (2.42, 180)$.

To also compare computational expense, the times it took for integrations to reach the end and for indicators to reach break value are given below.

Type	t
plain orbit (no veqs)	18.11s
plain orbit (w/ veqs)	44.29s
LCN	44.60s
DFLI	44.29s
MEGNO	44.47s
SALI	*70.21s
RLI	89.51s ($\approx 2x$ LCN)

Table 5.3. Time to fully integrate orbits. Compare with integrating orbit without computing an indicator and without computing the variational equations.

Indicator	Threshold	t_k	Alt. threshold	t_k
DFLI	30	NaN	t	5.15000e+03
MEGNO	7	4.43600e+03	2	2.24000e+02
SALI	10^{-4}	7.69000e+02		
RLI	10^{-4}	8.45000e+02		

Table 5.4. Simulation time till breakvalue. Also in case of theoretical breakvalues for FLI and MEGNO.

About the dynamics, for the system to be stable planet d has to be significantly distant from planets b, c so orbits won't intersect. We note that planet can exist in stable anti-aligned position at $M = \pi \text{ rad} = 180 \text{ deg}$ if $a \gtrsim 2.45$.

Setting $M_d = \pi \text{ rad}$ we generate $a_d - e_d$ stability maps for $a_d \in [1.5, 3.0]$, $e_d \in [0.001, 0.5]$. The maps are shown for times 10^4 years.

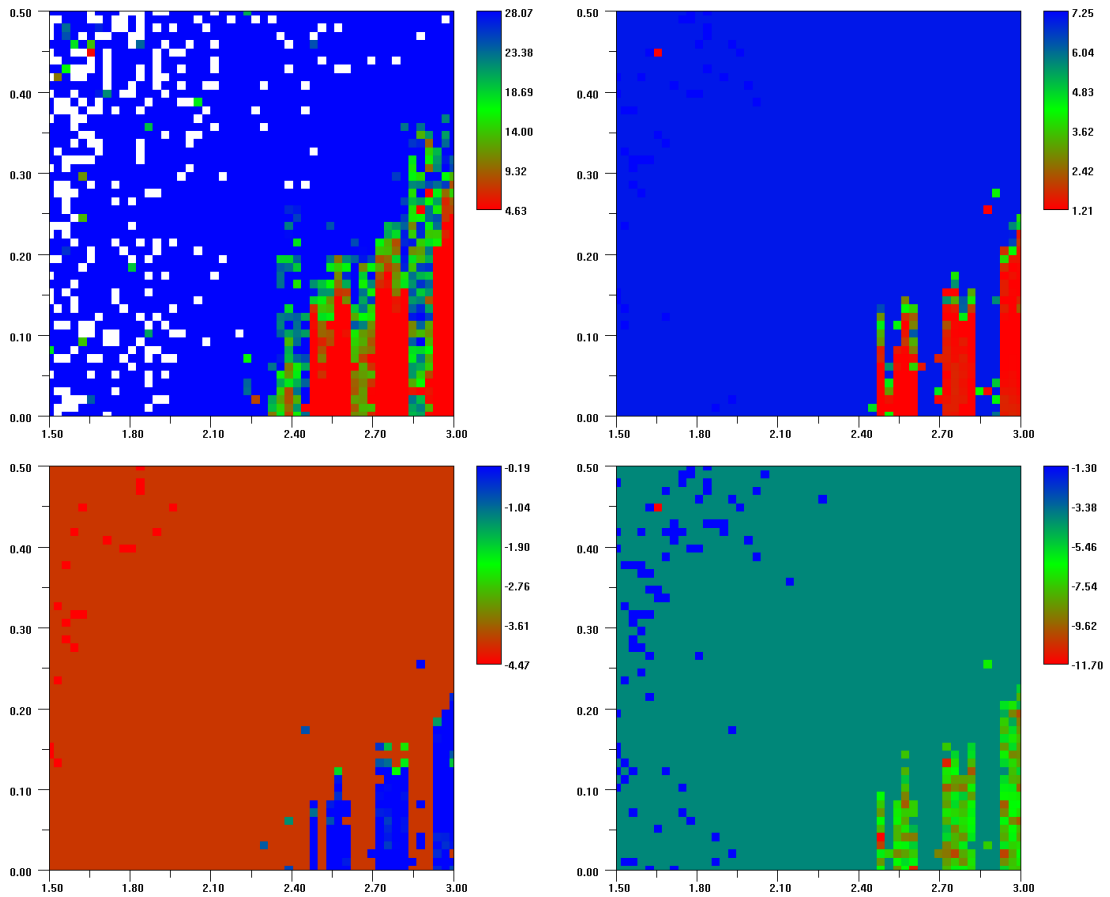


Figure 5.6. (top) DFLI left, MEGNO right, (bottom) log SALI left, log RLI right. The white spots show when integration has failed, i.e., a collision has occurred. The (x, y) axis are (a_d, e_d) respectively.

We choose the following regular and chaotic parameters.

Type	a_d	e_d
regular	2.52	0.02
chaotic	2.52	0.1

Table 5.5. Regular and chaotic orbit for $M_d=180.0$.

The evolution of a, e ($i = \text{const.}$) for regular orbit is

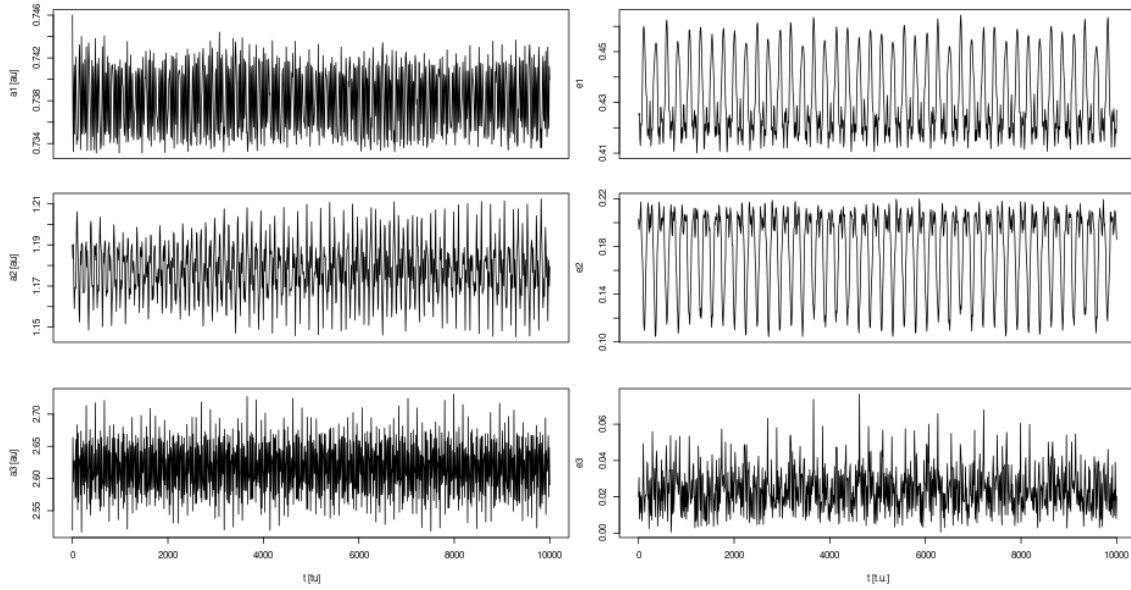


Figure 5.7. Evolution of a, e for regular orbit $(a_d, e_d) = (2.52, 0.02)$.

The evolution of a, e ($i = \text{const.}$) for chaotic orbit is

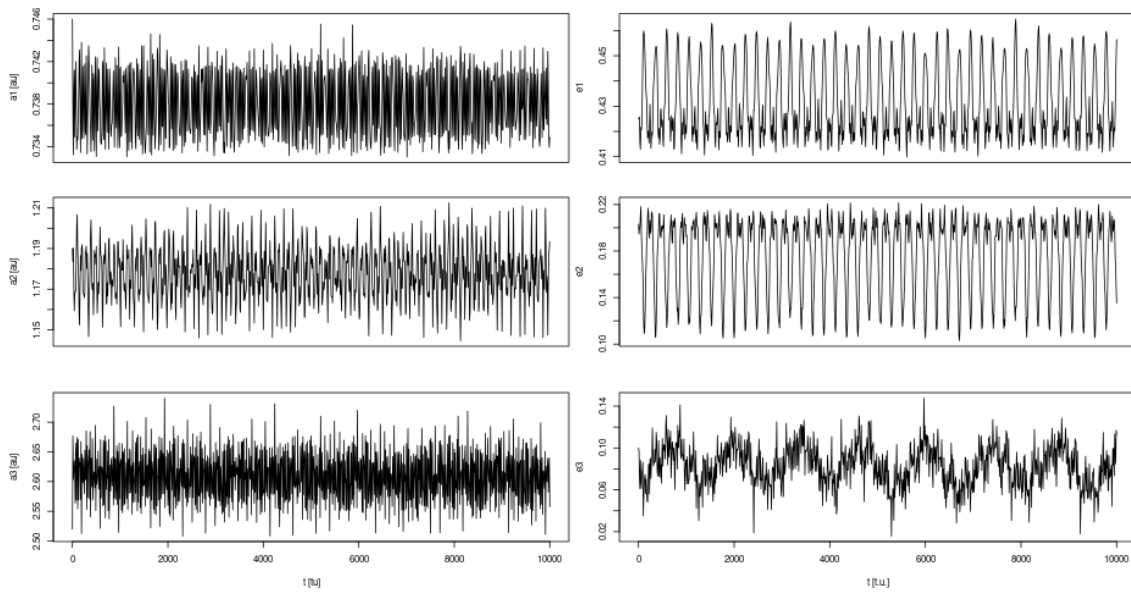


Figure 5.8. Evolution of a, e for chaotic orbit $(a_d, e_d) = (2.52, 0.1)$.

The evolution of the indicators is then taken to the end without early breaking in the case of chaotic orbit.

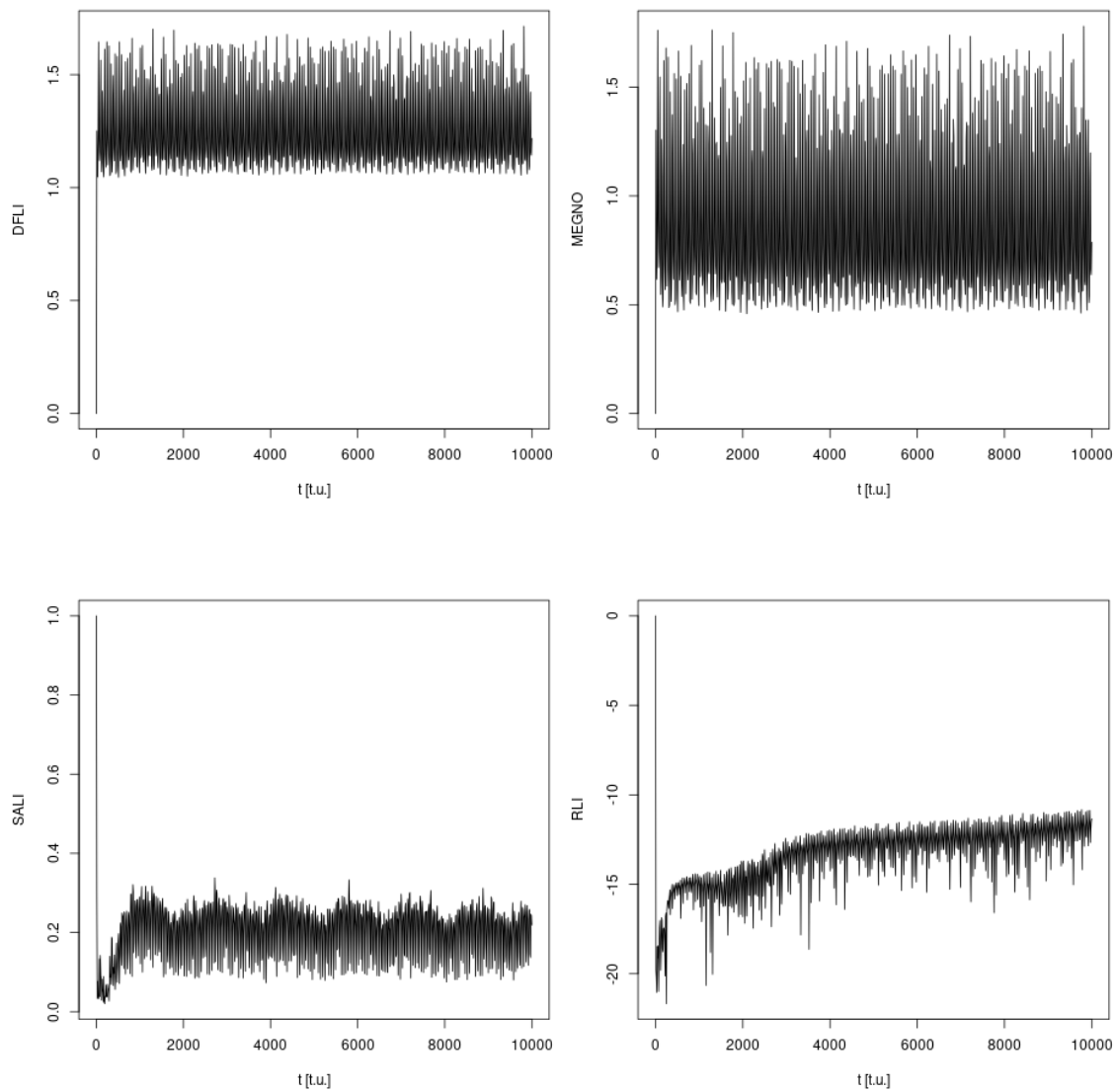


Figure 5.9. Evolution of DFLI, MEGNO, SALI, log RLI for regular orbit $(a_d, e_d) = (2.52, 0.02)$.

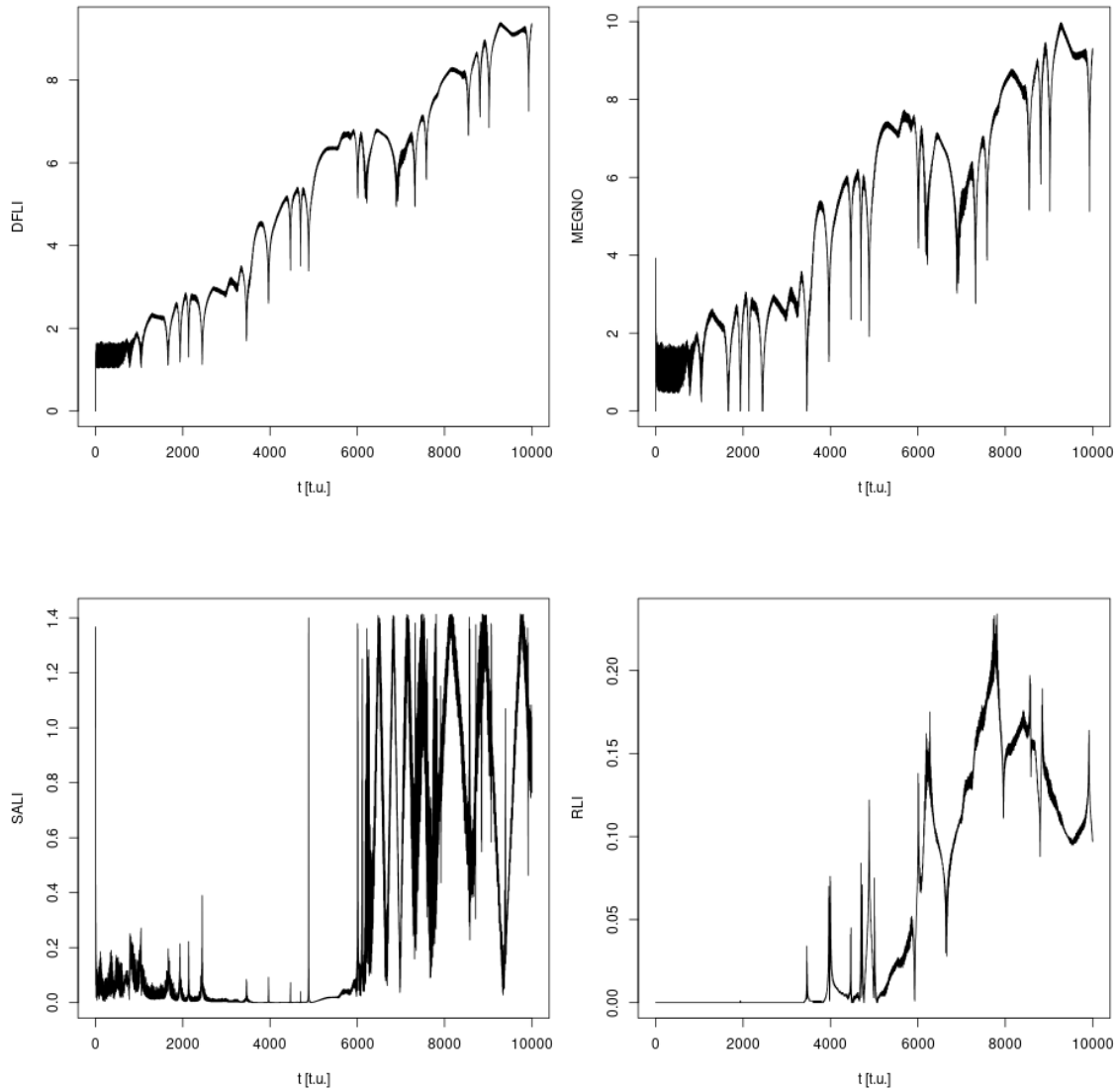


Figure 5.10. Evolution of DFLI, MEGNO, SALI, RLI for for chaotic orbit $(a_d, e_d) = (2.52, 0.1)$.

To also compare computational expense, the times it took for integrations to reach the end and for indicators to reach break value are given below.

Indicator	Threshold	t_k	Alt. threshold	t_k
DFLI	30	NaN	t	9.17000e+03
MEGNO	7	5.11300e+03	2	9.46000e+02
SALI	10^{-4}	3.59000e+03		
RLI	10^{-4}	1.93300e+03		

Table 5.6. Simulation time till breakvalue. Also in case of theoretical breakvalues for FLI and MEGNO.

The RLI, SALI can give very fast results (in iterations) but is reminded their higher computational complexity. SALI shows some strange behavior some time after reaching the

theoretical value 0. A possible explanation is accumulation of numerical errors, although something strange isn't seen in other indicators.

For MEGNO a higher threshold than theoretical value was chosen since it tends asymptotically to 2 but can oscillate slightly above or below in finite times. It's worth pointing its very close behavior to DFLI. Both indicators show oscillation around some value for regular orbits and linear increase for chaotic. This is distinct from plain FLI that for regular orbits shows logarithmic increase.

For the maps we've chosen a high DFLI value which value though is often used for longer integration times (>100 ky). If the theoretical threshold t is used we find that it gives results in same time span as MEGNO.

Overall, all indicators show strengths and weaknesses. DFLI being very simple to implement but requiring a good threshold choice, MEGNO having a slightly higher complexity but having the strong advantage of providing a theoretical max value (though for which we still have to consider oscillations that can put an orbit higher than it), SALI, and RLI being very fast but having higher complexity requiring evolution of two deviation vectors and two orbits respectively as well as choosing a good threshold.

Overall, a low mass 3rd planet introduced to the strongly resonant 2-planet system HD 82943, for short orbital distances, has regular orbits only for anti-aligned position and having low eccentricity. If orbital distance increases enough then there are stability regions for any starting position as long as eccentricity stays low but we notice chaoticity regions interwinding with them^{5.5}. At those chaoticity regions (for specific orbital distances) the planet d is in near-resonance with one of the inner planets. Finally, interestingly in both chaotic cases examined the system remained stable in the studied time span. Hence future research paths could be (i) exploring the chaoticity regions appearing inbetween stability regions, and (ii) exploring the prediction of stable and unstable chaos.

^{5.5} Ruminant of Kirkwood gaps found in the distribution of the semi-major axes of the orbits of main-belt asteroids.

CONCLUSIONS

Summing up, we presented the necessary background in (i) dynamical systems and numerical integration schemes, (ii) the planetary problem and its equations of motion, (iii) the variational equations of the previous problem, (iv) chaos indicators.

We showed some examples of the presented theory in every theoretical chapter, and how the equations required for studying those examples can be extracted computationally using the computer algebra system Maxima.

Finally we run numerical integrations for the system HD 82943 to compare the indicators in accuracy and performance. The comparison was made making stability maps for initial conditions of dynamical parameters of the outer planet. The indicators compared were DFLI, MEGNO, SALI, and RLI. Although the OFLI was presented in theory it was excluded because it has same behavior with FLI except the case of periodic orbits. Our results showed all indicators have strengths and weaknesses.

On the dynamics of the 3-planet system, we showed how introduction of 3rd planet modifies the dynamics of the planetary system and how changes in dynamical parameters of the outer body in the 3-planet system changes the stability of the orbits of the system with some parameters resulting in regular and some in chaotic motion. That is order and chaos co-exist in the N -body problem.

APPENDIX A

SOURCES

A.1. VARIATIONAL EQUATIONS

A partial extract from the in-house program, written in C, to showcase the utilized method. As already mentioned, for this thesis the code was modified by the author of this thesis from 2-planet to the 3-planet problem^{A.1}.

The array `y[]` (of size $2 \times 6n + 1 = 37$ in case of $n = 3$) contains time, and components of the position and velocity of primary and variational equations. Essentially it represents the vector

$$\mathbf{y} = (t, x_1, x_2, x_3, y_1, \dots, z_3, \dot{x}_1, \dot{x}_2, \dot{x}_3, \dot{y}_1, \dots, \dot{z}_3, \delta x_1, \delta x_2, \delta x_3, \delta y_1, \dots, \delta z_3, \delta \dot{x}_1, \delta \dot{x}_2, \delta \dot{x}_3, \delta \dot{y}_1, \dots, \delta \dot{z}_3)$$

The array `dd[]` contains the differential equations of the system with respect to `y[]`. Essentially it represents the vector

$$\frac{d\mathbf{y}}{dt} = (1, \dot{x}_1, \dot{x}_2, \dot{x}_3, \dot{y}_1, \dots, \dot{z}_3, \ddot{x}_1, \ddot{x}_2, \ddot{x}_3, \ddot{y}_1, \dots, \ddot{z}_3, \delta \dot{x}_1, \delta \dot{x}_2, \delta \dot{x}_3, \delta \dot{y}_1, \dots, \delta \dot{z}_3, \delta \ddot{x}_1, \delta \ddot{x}_2, \delta \ddot{x}_3, \delta \ddot{y}_1, \dots, \delta \ddot{z}_3)$$

The variational equations are implemented in form $\dot{\mathbf{w}} = \mathbf{P} \cdot \mathbf{w}$, $\mathbf{P} = \mathbf{A} + \mathbf{B}$, as presented in theory. Note the order of rows is different due to order of components differing.

```

void dSystem4BPveq(__attribute__((unused)) double t, double y[], double
dd[])
{
    //0th body
    double
        sx0=-(m1*y[1]+m2*y[2]+m3*y[3])/m0,
        sy0=-(m1*y[4]+m2*y[5]+m3*y[6])/m0,
        sz0=-(m1*y[7]+m2*y[8]+m3*y[9])/m0;
    //differences xi-xj
    double
        wx12=y[1]-y[2], wx13=y[1]-y[3], wx23=y[2]-y[3],
        wy12=y[4]-y[5], wy13=y[4]-y[6], wy23=y[5]-y[6],
        wz12=y[7]-y[8], wz13=y[7]-y[9], wz23=y[8]-y[9],
        wx10=y[1]-sx0, wx20=y[2]-sx0, wx30=y[3]-sx0,
        wy10=y[4]-sy0, wy20=y[5]-sy0, wy30=y[6]-sy0,
        wz10=y[7]-sz0, wz20=y[8]-sz0, wz30=y[9]-sz0;
    //distances - powers
    //r^2
    double
        r12=wx12*wx12+wy12*wy12+wz12*wz12,
        r13=wx13*wx13+wy13*wy13+wz13*wz13,
        r23=wx23*wx23+wy23*wy23+wz23*wz23,
        r10=wx10*wx10+wy10*wy10+wz10*wz10,

```

A.1. An N -body variant, utilizing a symplectic map, is detailed in [9].

```

    r202=wx20*wx20+wy20*wy20+wz20*wz20,
    r302=wx30*wx30+wy30*wy30+wz30*wz30;
//r
double
    r12=sqrt(r122), r13=sqrt(r132), r23=sqrt(r232),
    r10=sqrt(r102), r20=sqrt(r202), r30=sqrt(r302);
//r^(-3), 3*r^(-5)
double
    ir123=1.0/(r122*r12), ir133=1.0/(r132*r13), ir233=1.0/(r232*r23),
    ir125=3.0*ir123/r122, ir135=3.0*ir133/r132, ir235=3.0*ir233/r232,
    ir103=1.0/(r102*r10), ir203=1.0/(r202*r20), ir303=1.0/(r302*r30),
    ir105=3.0*ir103/r102, ir205=3.0*ir203/r202, ir305=3.0*ir303/r302;

//Differential equations of 1st ORDER
//xdi=vi
dd[1]=y[10];
dd[2]=y[11];
dd[3]=y[12];
dd[4]=y[13];
dd[5]=y[14];
dd[6]=y[15];
dd[7]=y[16];
dd[8]=y[17];
dd[9]=y[18];
//vdi=-sum(mj*wxij*irij3)
dd[10]=-m0*wx10*ir103-m2*wx12*ir123-m3*wx13*ir133;
dd[11]=-m0*wx20*ir203+m1*wx12*ir123-m3*wx23*ir233;
dd[12]=-m0*wx30*ir303+m1*wx13*ir133+m2*wx23*ir233;
dd[13]=-m0*wy10*ir103-m2*wy12*ir123-m3*wy13*ir133;
dd[14]=-m0*wy20*ir203+m1*wy12*ir123-m3*wy23*ir233;
dd[15]=-m0*wy30*ir303+m1*wy13*ir133+m2*wy23*ir233;
dd[16]=-m0*wz10*ir103-m2*wz12*ir123-m3*wz13*ir133;
dd[17]=-m0*wz20*ir203+m1*wz12*ir123-m3*wz23*ir233;
dd[18]=-m0*wz30*ir303+m1*wz13*ir133+m2*wz23*ir233;
//-----
//veqs    vdot=P.v, P=A+B;
//-----
//row -> (j,b)=(0,0),(1,0),(2,0),(0,1),... (j the mass on the row)
//col -> (i,a)=(0,0),(1,0),(2,0),(0,1),...
double B[9][9]; // Matrix B
double
    bxx12=-ir123+wx12*wx12*ir125, byy12=-ir123+wy12*wy12*ir125, bzz12=-
ir123+wz12*wz12*ir125,
    bxy12=wx12*wy12*ir125, bxz12=wx12*wz12*ir125,
byz12=wy12*wz12*ir125,
    bxx13=-ir133+wx13*wx13*ir135, byy13=-ir133+wy13*wy13*ir135, bzz13=-
ir133+wz13*wz13*ir135,
    bxy13=wx13*wy13*ir135, bxz13=wx13*wz13*ir135,
byz13=wy13*wz13*ir135,
    bxx23=-ir233+wx23*wx23*ir235, byy23=-ir233+wy23*wy23*ir235, bzz23=-
ir233+wz23*wz23*ir235,

```

```

    bxy23=wx23*wy23*ir235, bxz23=wx23*wz23*ir235,
    byz23=wy23*wz23*ir235;

    //-----
    double A[9][9]; // Matrix A
    double
        m01=m0+m1, m02=m0+m2, m03=m0+m3;
    double
        txx1=-ir103+wx10*wx10*ir105, txx2=-ir203+wx20*wx20*ir205, txx3=-
    ir303+wx30*wx30*ir305,
        tyy1=-ir103+wy10*wy10*ir105, tyy2=-ir203+wy20*wy20*ir205, tyy3=-
    ir303+wy30*wy30*ir305,
        tzz1=-ir103+wz10*wz10*ir105, tzz2=-ir203+wz20*wz20*ir205, tzz3=-
    ir303+wz30*wz30*ir305;
    double
        txy1=wx10*wy10*ir105, txy2=wx20*wy20*ir205, txy3=wx30*wy30*ir305,
        txz1=wx10*wz10*ir105, txz2=wx20*wz20*ir205, txz3=wx30*wz30*ir305,
        tyz1=wy10*wz10*ir105, tyz2=wy20*wz20*ir205, tyz3=wy30*wz30*ir305;

    //xx; (0,0)
    A[0][0]=m01*txx1; A[0][1]=m2*txx1; A[0][2]=m3*txx1;
    A[1][0]=m1*txx2; A[1][1]=m02*txx2; A[1][2]=m3*txx2;
    A[2][0]=m1*txx3; A[2][1]=m2*txx3; A[2][2]=m03*txx3;
    //yy; (1,1)
    A[3][3]=m01*tyy1; A[3][4]=m2*tyy1; A[3][5]=m3*tyy1;
    A[4][3]=m1*tyy2; A[4][4]=m02*tyy2; A[4][5]=m3*tyy2;
    A[5][3]=m1*tyy3; A[5][4]=m2*tyy3; A[5][5]=m03*tyy3;
    //zz; (2,2)
    A[6][6]=m01*tzz1; A[6][7]=m2*tzz1; A[6][8]=m3*tzz1;
    A[7][6]=m1*tzz2; A[7][7]=m02*tzz2; A[7][8]=m3*tzz2;
    A[8][6]=m1*tzz3; A[8][7]=m2*tzz3; A[8][8]=m03*tzz3;
    //xy; (0,1)&(1,0)
    A[0][3]=A[3][0]=m01*txy1; A[0][4]=A[3][1]=m2*txy1;
    A[0][5]=A[3][2]=m3*txy1;
    A[1][3]=A[4][0]=m1*txy2; A[1][4]=A[4][1]=m02*txy2;
    A[1][5]=A[4][2]=m3*txy2;
    A[2][3]=A[5][0]=m1*txy3; A[2][4]=A[5][1]=m2*txy3;
    A[2][5]=A[5][2]=m03*txy3;
    //xz; (0,2)&(2,0)
    A[0][6]=A[6][0]=m01*txz1; A[0][7]=A[6][1]=m2*txz1;
    A[0][8]=A[6][2]=m3*txz1;
    A[1][6]=A[7][0]=m1*txz2; A[1][7]=A[7][1]=m02*txz2;
    A[1][8]=A[7][2]=m3*txz2;
    A[2][6]=A[8][0]=m1*txz3; A[2][7]=A[8][1]=m2*txz3;
    A[2][8]=A[8][2]=m03*txz3;
    //yz; (1,2)&(2,1)
    A[3][6]=A[6][3]=m01*tyz1; A[3][7]=A[6][4]=m2*tyz1;
    A[3][8]=A[6][5]=m3*tyz1;
    A[4][6]=A[7][3]=m1*tyz2; A[4][7]=A[7][4]=m02*tyz2;
    A[4][8]=A[7][5]=m3*tyz2;

```

```

    A[5][6]=A[8][3]=m1*tyz3; A[5][7]=A[8][4]=m2*tyz3;
A[5][8]=A[8][5]=m03*tyz3;

    for(int i=0;i<9;i++) for(int j=0;j<9;j++) A[i][j]+=B[i][j];
    //A becomes the total matrix

    for(int i=19;i<28;i++) dd[i]=y[i+9];
    for(int i=0;i<9;i++){
        double sum=0;
        for(int j=0;j<9;j++) sum+=A[i][j]*y[19+j];
        dd[28+i]=sum;
    }
}

```

A.2. CHAOS INDICATORS

Similar to previous, for this thesis the code was partially modified by the author of this thesis. Specifically based on already existent MLCN and FLI code, subroutines for all were made. This will show the slight implementation difference for the computation of those indicators.

The subroutines take as input an array $x0[]$ corresponding to \mathbf{y} shown previously and a pointer $*ptr_ci$ to a scalar value corresponding to the indicator computed and returns the iteration at which the integration ended. Each subroutine modifies this scalar to the final value of the indicator.

The global variables utilized across all are NNEQ, NEQ, Niters, DT that correspond to the number of differential equations of the primary system (or else the components of primary equations), the total number of differential equations (or else the components) when including the variational, the total number of integration steps, and the integration time step. Those variables NNEQ, NEQ were defined because code is modifiable to also include mass as parameters and in case program is run with an N -body integration class. The breakvalues for each indicator are also defined as global variables. Those are the self-explained LCN_BREAKVAL, DFLIMAX, MEGNOMAX, SALI_BREAKVAL, RLI_BREAKVAL. There's also RLI_SEP that sets the distance of shadow orbit modifying $y[1]$ (essentially x_1).

The `vsys.DTstep(yin[],DT,*dt,yout[])` performs an integration step for $y_{in} = y(t)$ populating $y_{out} = y(t + DT)$. The value `dt` sets the minimum integration time and is varied as explained in theory for the B.-S. integrator.

```

int GetLCN(double x0[], double *ptr_lcn)
{
    double X0[NEQ], X1[NEQ];
    for(int j=0;j<NNEQ;j++) X0[j]=x0[j];
    X0[0]=0.0;
    int k;
    double dt=0.01, ksi=0, intdt=0, lcn;
    for(int j=NNEQ;j<NEQ;j++) X0[j]=0;
    X0[NNEQ]=1;
    for(k=1;k<=Niters;k++)
    {
        if(!vsys.DTstep(X0,DT,&dt,X1)) {
            *ptr_lcn=1.0/k;
            return k;
        }
    }
}

```

```

    }

    ksi=0;
    for(int j=NNEQ;j<NEQ;j++) ksi+=X1[j]*X1[j];
    ksi=sqrt(ksi);

    intdt+=log10(ksi);
    lcn=log10(intdt/X1[0]);
    //if(lcn<LCN_BREAKVAL) break;

    for(int j=0;j<NNEQ;j++) XO[j]=X1[j];
    for(int j=NNEQ;j<NEQ;j++) XO[j]=X1[j]/ksi;
}
*ptr_lcn=lcn;
return k;
}

```

For the FLI there's a choice between taking as initial conditions for deviation vector $v_0^{(1)} = 1, v_0^{(i)} = 0, i > 1$ that is $\mathbf{v}_0 = (1, 0, 0, \dots, 0)$ or tangent to the orbit via $\dot{\mathbf{x}} / \|\dot{\mathbf{x}}\|$. Of course that part can be applied to others indicators. It's only here because was used to test whether different initial condition for deviation vector resulted in different dynamical results, something that we found wasn't the case.

```

int GetDFLI(double x0[], double *dfli)
{
    double XO[NEQ], X1[NEQ];
    for(int j=0;j<NNEQ;j++) XO[j]=x0[j];
    XO[0]=0.0;
    int k;
    double dt=0.01, ksi=0, flisup=-DFLIMAX, fli; //init val
    //GetDV{
    //simple deviation vector choice
    for(int j=NNEQ;j<NEQ;j++) XO[j]=0;
    XO[NNEQ]=1;
    //deviation vector tangent to flow at t0
    //for(int j=1;j<NNEQ;j++) ksi+=XO[j]*XO[j];
    //ksi=sqrt(ksi);
    //for(int j=NNEQ;j<NEQ;j++) XO[j]=XO[j-NNEQ]/ksi;
    //}
    for(k=1;k<=Niters;k++)
    {
        if(!vsys.DTstep(XO,DT,&dt,X1)) {
            //*dfli=DFLIMAX;
            *dfli=31;
            return k;
        }

        ksi=0;
        for(int j=NNEQ;j<NEQ;j++) ksi+=X1[j]*X1[j];
        ksi=sqrt(ksi);
    }
}

```

```

        fli=log10(ksi/X1[0]);
        if(flisup<fli) flisup=fli;
        if(fli>DFLIMAX) {
            *dfli=DFLIMAX-1;
            return k;
        }

        for(int j=0;j<NEQ;j++) X0[j]=X1[j];
    }
    *dfli=flisup;
    return k;
}

int GetMEGNO(double x0[], double *ptr_mgn)
{
    double X0[NEQ], X1[NEQ];
    for(int j=0;j<NNEQ;j++) X0[j]=x0[j];
    X0[0]=0.0;
    int k;
    double dt=0.01, ksi=0, intdt=0, mgn;
    for(int j=NNEQ;j<NEQ;j++) X0[j]=0;
    X0[NNEQ]=1;
    for(k=1;k<=Niters;k++)
    {
        if(!vsys.DTstep(X0,DT,&dt,X1)) {
            *ptr_mgn=MEGNOMAX+1;
            return k;
        }

        ksi=0;
        for(int j=NNEQ;j<NEQ;j++) ksi+=X1[j]*X1[j];
        ksi=sqrt(ksi);

        intdt+=log10(ksi)*X1[0];
        mgn=intdt*2/X1[0];
        if(mgn>MEGNOMAX) {
            *ptr_mgn=MEGNOMAX;
            return k;
        }

        for(int j=0;j<NNEQ;j++) X0[j]=X1[j];
        for(int j=NNEQ;j<NEQ;j++) X0[j]=X1[j]/ksi;
    }
    *ptr_mgn=mgn;
    return k;
}

```

For the SALI we used a sub-optimal implementation for simplicity. Specifically we're evolving two orbits rather than including an extra set of variational equations to evolve only two deviation vectors as shown in example for HH. For the times we considered this and subtract the time that takes to evolve a second orbit.


```

int GetSALI(double x0[], double *ptr_sali)
{
    double XO[NEQ], YO[NEQ], X1[NEQ], Y1[NEQ], XY[NEQ];
    for(int j=0;j<NNEQ;j++) XO[j]=x0[j];
    for(int j=0;j<NNEQ;j++) YO[j]=x0[j];
    XO[0]=YO[0]=0.0;
    int k;
    double dt=0.01, ksi=0, sali, a, b;
    for(int j=NNEQ;j<NEQ;j++) XO[j]=0;
    for(int j=NNEQ;j<NEQ;j++) YO[j]=0;
    XO[NNEQ]=YO[NNEQ+3]=1;
    for(k=1;k<=Niters;k++)
    {
        if(!vsys.DTstep(XO,DT,&dt,X1)) {
            *ptr_sali=0.0;
            return k;
        }
        if(!vsys.DTstep(YO,DT,&dt,Y1)) {
            *ptr_sali=0.0;
            return k;
        }

        //normalize u_1
        ksi=0;
        for(int j=NNEQ;j<NEQ;j++) ksi+=X1[j]*X1[j];
        ksi=sqrt(ksi);
        for(int j=NNEQ;j<NEQ;j++) X1[j]=X1[j]/ksi;

        //normalize u_2
        ksi=0;
        for(int j=NNEQ;j<NEQ;j++) ksi+=Y1[j]*Y1[j];
        ksi=sqrt(ksi);
        for(int j=NNEQ;j<NEQ;j++) Y1[j]=Y1[j]/ksi;

        //compute ||u_1-u_2||
        for(int j=NNEQ;j<NEQ;j++) XY[j]=X1[j]-Y1[j];
        ksi=0;
        for(int j=NNEQ;j<NEQ;j++) ksi+=XY[j]*XY[j];
        a=sqrt(ksi);

        //compute ||u_1+u_2||
        for(int j=NNEQ;j<NEQ;j++) XY[j]=X1[j]+Y1[j];
        ksi=0;
        for(int j=NNEQ;j<NEQ;j++) ksi+=XY[j]*XY[j];
        b=sqrt(ksi);

        //find min(...)
        sali=a<b?a:b;
        if(sali<SALI_BREAKVAL) {
            *ptr_sali=SALI_BREAKVAL;
        }
    }
}

```

```

        return k;
    }

    for(int j=0;j<NEQ;j++) XO[j]=X1[j];
    for(int j=0;j<NEQ;j++) YO[j]=Y1[j];
}
*ptr_sali=sali;
return k;
}

int GetRLI(double x0[], double *ptr_rli)
{
    double XO[NEQ], SXO[NEQ], X1[NEQ], SX1[NEQ];
    for(int j=0;j<NNEQ;j++) XO[j]=x0[j];
    for(int j=0;j<NNEQ;j++) SXO[j]=x0[j];
    XO[0]=SXO[0]=0.0;
    //simple separation
    SXO[1]=XO[1]+RLI_SEP;
    int k;
    double dt=0.01, ksi=0, intdt=0, intdts=0, lcn, lcns, dlc, rli;
    for(int j=NNEQ;j<NEQ;j++) XO[j]=0;
    for(int j=NNEQ;j<NEQ;j++) SXO[j]=0;
    XO[NNEQ]=SXO[NNEQ]=1;
    for(k=1;k<=Niters;k++)
    {
        if(!vsys.DTstep(XO,DT,&dt,X1)) {
            *ptr_rli=1.0;
            return k;
        }
        if(!vsys.DTstep(SXO,DT,&dt,SX1)) {
            *ptr_rli=1.0;
            return k;
        }
    }

    //normal orbit LCN compute and d.v.  normalize
    ksi=0;
    for(int j=NNEQ;j<NEQ;j++) ksi+=X1[j]*X1[j];
    ksi=sqrt(ksi);

    intdt+=log10(ksi);
    lcn=log10(intdt/X1[0]);

    for(int j=NNEQ;j<NEQ;j++) XO[j]=X1[j]/ksi;

    //shadow orbit LCN compute and d.v.  normalize
    ksi=0;
    for(int j=NNEQ;j<NEQ;j++) ksi+=SX1[j]*SX1[j];
    ksi=sqrt(ksi);

    intdts+=log10(ksi);
    lcns=log10(intdts/SX1[0]);
}

```

```
    for(int j=NNEQ;j<NEQ;j++) SX0[j]=SX1[j]/ksi;

    dlcn=abs(lcn-lcns);
    rli=dlcn;
    if(rli>RLI_BREAKVAL) {
        *ptr_rli=RLI_BREAKVAL;
        return k;
    }

    for(int j=0;j<NNEQ;j++) XO[j]=X1[j];
    for(int j=0;j<NNEQ;j++) SX0[j]=SX1[j];
}
*ptr_rli=rli;
return k;
}
```


BIBLIOGRAPHY

- [1] G. Voyatzis and E. Meletlidou. *Εισαγωγή στα μη γραμμικά δυναμικά συστήματα*. Kallipos, Open Academic Editions.
- [2] J. Meiss. Dynamical systems. *Scholarpedia*, 2(2):1629, 2007. Revision #197505.
- [3] J. Meiss. Hamiltonian systems. *Scholarpedia*, 2(8):1943, 2007. Revision #197503.
- [4] Vladimir I Arnol'd. Small denominators and problems of stability of motion in classical and celestial mechanics. *Russian Mathematical Surveys*, 18(6):85, 1963.
- [5] R.L. Devaney. *An Introduction To Chaotic Dynamical Systems, Second Edition*. Addison-Wesley advanced book program. Avalon Publishing, 1989.
- [6] John Banks, Jeffrey Brooks, Grant Cairns, Gary Davis, and Peter Stacey. On Devaney's definition of chaos. *The American mathematical monthly*, 99(4):332–334, 1992.
- [7] J. Stoer and R. Bulirsch. Ordinary differential equations. *Introduction to Numerical Analysis*, pages 404–535, 1980.
- [8] WH Press, BP Flannery, SA Teukolsky, and WT Vetterling. Richardson extrapolation and the Bulirsch-Stoer method. *Numerical Recipes in FORTRAN: The Art of Scientific Computing*, pages 718–725, 1992.
- [9] Dimitra Skoulidou. *Symplectic integration of equations of motion and variational equations for extrasolar systems of N-planets*. Msc thesis, Aristotle University, Thessaloniki, 9 2017.
- [10] Gerhard Beutler. The equations of motion. *Methods of Celestial Mechanics: Volume I: Physical, Mathematical, and Numerical Principles*, pages 45–121, 2005.
- [11] Gerhard Beutler. Variational equations. *Methods of Celestial Mechanics: Volume I: Physical, Mathematical, and Numerical Principles*, pages 175–207, 2005.
- [12] Ch Skokos and Enrico Gerlach. Numerical integration of variational equations. *Physical Review E*, 82(3):36704, 2010.
- [13] Hanno Rein and Daniel Tamayo. Second-order variational equations for N-body simulations. *Monthly Notices of the Royal Astronomical Society*, 459(3):2275–2285, 2016.
- [14] P. Holmes and E. T. Shea-Brown. Stability. *Scholarpedia*, 1(10):1838, 2006. Revision #137538.
- [15] Roman V. Baluev and C. Beaugé. Possible solution to the riddle of HD 82943 multiplanet system: the three-planet resonance 1:2:5? *Monthly Notices of the Royal Astronomical Society*, 439(1):673–689, 01 2014.
- [16] Javier Guillermo Marti, Cristian Andrés Giuppone, and Cristian Beauge. Dynamical analysis of the Gliese-876 Laplace resonance. *Monthly Notices of the Royal Astronomical Society*, 433(2):928–934, 2013.
- [17] G Tancredi, A Sánchez, and F Roig. A comparison between methods to compute Lyapunov exponents. *The Astronomical Journal*, 121(2):1171, 2001.
- [18] Ch Skokos. The Lyapunov characteristic exponents and their computation. In *Dynamics of Small Solar System Bodies and Exoplanets*, pages 63–135. Springer, 2009.
- [19] Claude Froeschlé, R. Gonczi, and Elena Lega. The fast Lyapunov indicator: a simple tool to detect weak chaos. Application to the structure of the main asteroidal belt. *Planetary and Space Science*, 45(7):881–886, 1997. Asteroids, Comets, Meteors 1996 - II.
- [20] Elena Lega, Massimiliano Guzzo, and Claude Froeschlé. Theory and Applications of the Fast Lyapunov Indicator (FLI) Method. Pages 35–54, 2016.
- [21] Claude Froeschlé and Elena Lega. On the structure of symplectic mappings. the fast lyapunov indicator: a very sensitive tool. In *New Developments in the Dynamics of Planetary Systems: Proceedings of the Fifth Alexander von Humboldt Colloquium on Celestial Mechanics held in Badhofgastein (Austria), 19–25 March 2000*, pages 167–195. Springer, 2001.
- [22] Nicolás Pablo Maffione, Luciano A Darriba, Pablo M Cincotta, and Claudia M Giordano. A comparison of different indicators of chaos based on the deviation vectors: application to symplectic mappings. *Celestial Mechanics and Dynamical Astronomy*, 111:285–307, 2011.
- [23] Luciano A Darriba, Nicolás Pablo Maffione, Pablo M Cincotta, and Claudia M Giordano. Comparative study of variational chaos indicators and ODEs' numerical integrators. *International Journal of Bifurcation and Chaos*, 22(10):1230033, 2012.
- [24] Zsolt Sándor and Nicolás Maffione. *The Relative Lyapunov Indicators: Theory and Application to Dynamical Astronomy*, pages 183–220. Springer Berlin Heidelberg, Berlin, Heidelberg, 2016.

- [25] Elena Lega and Claude Froeschlé. On the relationship between fast lyapunov indicator and periodic orbits for symplectic mappings. In *Dynamics of Natural and Artificial Celestial Bodies: Proceedings of the US/European Celestial Mechanics Workshop, held in Poznań, Poland, 3–7 July 2000*, pages 129–147. Springer, 2001.
- [26] George Voyatzis. Chaos, order, and periodic orbits in 3:1 resonant planetary dynamics. *The Astrophysical Journal*, 675(1):802, mar 2008.
- [27] Marc Fouchard, Elena Lega, Christiane Froeschlé, and Claude Froeschlé. On the relationship between fast lyapunov indicator and periodic orbits for continuous flows. In *Modern Celestial Mechanics: From Theory to Applications: Proceedings of the Third Meeting on Celestial Mechanics—CELMEC III, held in Rome, Italy, 18–22 June, 2001*, pages 205–222. Springer, 2002.
- [28] Roberto Barrio. Theory and Applications of the Orthogonal Fast Lyapunov Indicator (OFLI and OFLI2) Methods. *Chaos Detection and Predictability*, pages 55–92, 2016.
- [29] Roberto Barrio. Sensitivity tools vs. poincaré sections. *Chaos, Solitons & Fractals*, 25(3):711–726, 2005.
- [30] Roberto Barrio, Wojtek Borczyk, and S Breiter. Spurious structures in chaos indicators maps. *Chaos, Solitons & Fractals*, 40(4):1697–1714, 2009.
- [31] P. M. Cincotta and C. Simó. Simple tools to study global dynamics in non-axisymmetric galactic potentials - I. *Astron. Astrophys. Suppl. Ser.*, 147(2):205–228, 2000.
- [32] P. M. Cincotta, C. M. Giordano, and C. Simó. Phase space structure of multi-dimensional systems by means of the mean exponential growth factor of nearby orbits. *Physica D: Nonlinear Phenomena*, 182(3):151–178, 2003.
- [33] P. M. Cincotta and C. M. Giordano. Theory and Applications of the Mean Exponential Growth Factor of Nearby Orbits (MEGNO) Method. *Chaos Detection and Predictability*, pages 93–128, 2016.
- [34] M. F. Mestre, P. M. Cincotta, and C. M. Giordano. Analytical relation between two chaos indicators: FLI and MEGNO. *Monthly Notices of the Royal Astronomical Society: Letters*, 414(1):0, 06 2011.
- [35] Charalampos (Haris) Skokos. Alignment indices: a new, simple method for determining the ordered or chaotic nature of orbits. *Journal of Physics A: Mathematical and General*, 34(47):10029, nov 2001.
- [36] Charalampos (Haris) Skokos and Thanos Manos. The Smaller (SALI) and the Generalized (GALI) Alignment Indices: Efficient Methods of Chaos Detection. *Chaos Detection and Predictability*, pages 129–181, 2016.
- [37] Ch Skokos, TC Bountis, and Ch Antonopoulos. Geometrical properties of local dynamics in Hamiltonian systems: The Generalized Alignment Index (GALI) method. *Physica D: Nonlinear Phenomena*, 231(1):30–54, 2007.
- [38] Zsolt Sándor, Bálint Érdi, András Széll, and Barbara Funk. The relative Lyapunov indicator: an efficient method of chaos detection. *Celestial Mechanics and Dynamical Astronomy*, 90:127–138, 2004.
- [39] Euaggelos E Zotos. Classifying orbits in the classical Hénon–Heiles Hamiltonian system. *Nonlinear Dynamics*, 79:1665–1677, 2015.
- [40] Vasilis Choustoulakis. *Αριθμητική μελέτη της δυναμικής ευστάθειας ταλαντωτών υπό την επίδραση περιοδικών, ημιπεριοδικών και χαοτικών διαταραχών*. Bsc thesis, Aristotle University, Thessaloniki, 7 2022.
- [41] C. Beaugé, C. A. Giuppone, Sylvio Ferraz-Mello, and Tatiana Alexandrovna Michtchenko. Reliability of orbital fits for resonant extrasolar planetary systems: the case of HD82943. *Monthly Notices of the Royal Astronomical Society*, 385(4):2151–2160, 2008.
- [42] Xianyu Tan, Matthew J Payne, Man Hoi Lee, Eric B Ford, Andrew W Howard, John A Johnson, Geoff W Marcy, and Jason T Wright. Characterizing the orbital and dynamical state of the HD 82943 planetary system with Keck radial velocity data. *The Astrophysical Journal*, 777(2):101, 2013.
- [43] Konstantinos Foutzopoulos. *Mean-motion resonances in exoplanetary systems*. Bsc thesis, Aristotle University, Thessaloniki, 10 2019.
- [44] Kyriaki I. Antoniadou. Regular and chaotic orbits in the dynamics of exoplanets. *The European Physical Journal Special Topics*, 225:1001–1016, 2016.
- [45] Kyriaki I. Antoniadou and George Voyatzis. Orbital stability of coplanar two-planet exosystems with high eccentricities. *Monthly Notices of the Royal Astronomical Society*, 461(4):3822–3834, 06 2016.